Inorganic Chemistry

Electronic Structure of Square Planar Bis(benzene-1,2-dithiolato)metal Complexes [M(L)₂]ᶻ (z = 2–, 1–, 0; M = Ni, Pd, Pt, Cu, Au): An Experimental, Density Functional, and Correlated ab Initio Study

Kallol Ray, Thomas Weyhermüller, Frank Neese,* and Karl Wieghardt*

Max-Planck-Institut für Bioanorganische Chemie, Stiftstrasse 34-36,
D-45470 Mülheim a. d. Ruhr, Germany

Received May 12, 2005

The three diamagnetic square planar complexes of nickel(II), palladium(II), and platinum(II) containing two S,S-coordinated 3,5-di-*tert*-butylbenzene-1,2-dithiolate ligands, $(L^{Bu})^{2-}$, namely $[M^{II}(L^{Bu})_2]^{2-}$, have been synthesized. The corresponding paramagnetic monoanions $[M^{II}(L^{Bu})(L^{Bu\bullet})]^-$ ($S = {}^1/_2$) and the neutral diamagnetic species $[M^{II}(L^{Bu\bullet})_2]$ (M = Ni, Pd, Pt) have also been generated in solution or in the solid state as $[N(n\text{-}Bu)_4][M^{II}(L^{Bu})(L^{Bu\bullet})]$ salts. The corresponding complex $[Cu^{III}(L^{Bu})_2]^-$ has also been investigated. The complexes have been studied by UV–vis, IR, and EPR spectroscopy and by X-ray crystallography; their electro- and magnetochemistry is reported. The electron-transfer series $[M(L^{Bu})_2]^{2-,-,0}$ is shown to be ligand based involving formally *one* $(L^{Bu\bullet})^-$ π radical in the monoanion or *two* in the neutral species $[M^{II}(L^{Bu\bullet})_2]$ (M = Ni, Pd, Pt). Geometry optimizations using all-electron density functional theory with scalar relativistic corrections at the second-order Douglas–Kroll–Hess (DKH2) and zeroth-order regular approximation (ZORA) levels result in excellent agreement with the experimentally determined structures and electronic spectra. For the three neutral species a detailed analysis of the orbital structures reveals that the species may best be described as containing two strongly antiferromagnetically interacting ligand radicals. Furthermore, multiconfigurational ab initio calculations using the spectroscopy oriented configuration interaction (SORCI) approach including the ZORA correction were carried out. The calculations predict the position of the intervalence charge-transfer band well. Chemical trends in the diradical characters deduced from the multiconfigurational singlet ground-state wave function along a series of metals and ligands were discussed.

Introduction

Since their discovery in 1963, square planar bis(benzene-1,2-dithiolato)metal complexes[1−5] have received considerable attention due to their interesting and often unusual electronic structures. Toluene-3,4-dithiolate, $(L^{Me})^{2-}$, and the unsubstituted derivative benzene-1,2-dithiolate, $(L)^{2-}$, have been used predominantly, but recently, Sellmann et al.[6] have introduced the sterically more demanding 3,5-di-*tert*-butyl-benzene-1,2-dithiolate ligand, $(L^{Bu})^{2-}$, and investigated its coordination chemistry with nickel.[7]

It has been established[2] that the square planar complexes $[M(L)_2]^{2-}$, $[M(L)_2]^-$, and $[M(L)_2]^0$ (M = Ni, Pt) form a three-membered electron-transfer series where the neutral species and the dianionic forms are diamagnetic with $S = 0$ ground states whereas the monoanions are paramagnetic ($S = {}^1/_2$). In contrast, the monoanion $[Cu(L^{Me})_2]^-$ possesses an $S = 0$ ground state[2] as does $[Au(L)_2]^-$,[3] whereas the corresponding dianions $[Cu(L^{Me})_2]^{2-}$ and $[Au(L)_2]^{2-}$ are paramagnetic ($S = {}^1/_2$) as is the neutral species $[Au(L^{Bu})_2]^0$.[8] Throughout the

* Authors to whom correspondence should be addressed. E-mail: wieghardt@mpi-muelheim.mpg.de (K.W.); neese@mpi-muelheim.mpg.de (F.N.).

(1) Reviews: (a) Schrauzer, G. N. *Transition Met. Chem.* **1968**, *4*, 299. (b) McCleverty, J. A. *Prog. Inorg. Chem.* **1968**, *10*, 49. (c) Holm, R. H.; O'Connor, M. J. *Prog. Inorg. Chem.* **1971**, *14*, 241. (d) Eisenberg, R. *Prog. Inorg. Chem.* **1970**, *12*, 295. (e) Gray, H. B. *Transition Met. Chem.* **1965**, *1*, 240. (f) *Dithiolene Chemistry*; Stiefel, E. I., Ed.; *Prog. Inorg. Chem.* **2004**, *52*.
(2) Gray, H. B.; Billig, E. *J. Am. Chem. Soc.* **1963**, *85*, 2019.
(3) Williams, R.; Billig, E.; Waters, J. H.; Gray, H. B. *J. Am. Chem. Soc.* **1966**, *88*, 43.
(4) Baker-Hawkes, M. J.; Billig, E.; Gray, H. B. *J. Am. Chem. Soc.* **1966**, *88*, 4870.
(5) Stiefel, E. I.; Waters, J. H.; Billig, E.; Gray, H. B. *J. Am. Chem. Soc.* **1965**, *87*, 3016.

(6) (a) Sellmann, D.; Freyberger, G.; Eberlein, R.; Böhlen, E.; Huttner, G.; Zsolnai, L. *J. Organomet. Chem.* **1987**, *323*, 21. (b) Sellmann, D.; Käppler, O. *Z. Naturforsch.* **1987**, *42b*, 1291.
(7) Sellmann, D.; Binder, H.; Häusinger, D.; Heinemann, F. W.; Sutter, J. *Inorg. Chim. Acta* **2000**, *300−302*, 829.
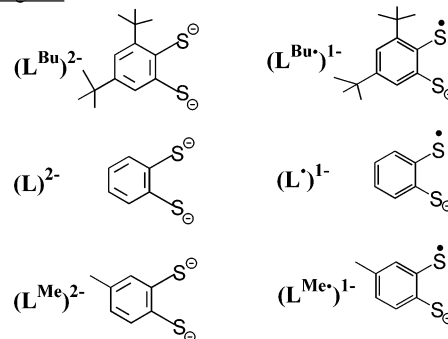
past 40 years there has been a debate on the nature of the electronic structure of these complexes. The question of ligand- vs metal-centered redox activity has led to diverse (and sometimes mutually exclusive) descriptions of the electronic structures of the members of an electron-transfer series.

As a recent example from the year 2000, consider the series $[Ni(L^{Bu})_2]^{0,-,2-}$ all of which have been characterized by X-ray crystallography (they are square planar) and by spectroscopy (UV−vis, EPR, XPS).[7] The authors concluded that "benzene-1,2-dithiolate(2−) and its $(L^{Bu})^{2-}$ derivative are normal 1,2-dithiolate(2−) ligands." This implies the occurrence of Ni^{II}, Ni^{III}, and Ni^{IV} in the di- and monoanion and in the neutral species, respectively. This interpretation had already been refuted[5] in 1965, where the radical character of the ligand in $[Ni^{II}(L^{Me\bullet})(L^{Me})]^-$ and $[Ni^{II}(L^{Me\bullet})_2]^0$ had been emphasized. In a recent correlated ab initio and density functional theoretical (DFT) investigation of diamagnetic $[Ni(L_N^{ISQ})_2]$, where $(L_N^{ISQ})^{\bullet-}$ represents the o-diiminobenzosemiquinonate(1−) π radical monoanion, we have shown[9a] that this species has ∼77% diradical character (from DDCI method). By using a broken symmetry DFT approach for the calculation of the electronic structure of the present sulfur containing $[Ni(L^{\bullet})_2]^0$ ($S = 0$) species, its diradical character has been estimated to be negligible (∼0%).[10] This is in agreement with previous DFT calculations.[11,12] We have now performed elaborate multireference post-Hartree−Fock ab initio calculations on the neutral complexes $[M(L^{\bullet})_2]^0$ (M = Ni, Pd, Pt) using the recently developed spectroscopy oriented configuration interaction (SORCI) method,[13] which is well suited for diradical species and will be used below to discuss the trends in the ground-state singlet wave functions along the series of complexes investigated.

Similarly, for diamagnetic $[Cu(L)_2]^-$ an electronic structure of (i) $[Cu^{III}(L)_2]^-$ containing a Cu^{III} ion (d[8], $S = 0$ in a square planar ligand environment) and two closed-shell dianions $(L)^{2-}$ has been proposed[2−4] or, alternatively, of (ii) $[Cu^{II}(L^{\bullet})(L)]^-$ has been proposed, where a monoanionic ligand π radical $(L^{\bullet})^-$ has been suggested to be intramolecularly antiferromagnetically coupled to a Cu^{II} (d[9]) ion.[14] It may be noted that the Goodenough−Kanamori rules for intramolecular spin exchange coupling between a π radical orbital and a $(d_{x^2-y^2})^1$ orbital of Cu^{II} would predict a ferromagnetic coupling yielding an $S = 1$ ground state[15] for the latter description because the two magnetic orbitals would be strictly orthogonal in a square planar CuS_4 unit. Recent

(8) Ray, K.; Weyhermüller, T.; Goossens, A.; Crajé, M. W. J.; Wieghardt, K. *Inorg. Chem.* **2003**, *42*, 4082.

(9) (a) Herebian, D.; Wieghardt, K.; Neese, F. *J. Am. Chem. Soc.* **2003**, *125*, 10997. (b) Herebian, D.; Bothe, E.; Neese, F.; Weyhermüller, T.; Wieghardt, K. *J. Am. Chem. Soc.* **2003**, *125*, 9116.

(10) Bachler, V.; Olbrich, G.; Neese, F.; Wieghardt, K. *Inorg. Chem.* **2002**, *41*, 4179.

(11) Lauterbach, C.; Fabian, J. *Eur. J. Inorg. Chem.* **1999**, 1995.

(12) Weber, J.; Daul, C.; von Zelewsky, A.; Goursot, A.; Penigault, E. *Chem. Phys. Lett.* **1982**, *88*, 78.

(13) Neese, F. *J. Chem. Phys.* **2003**, *119*, 9428.

(14) Sawyer, D. T.; Srivatsa, G. S.; Bodini, M. E.; Schaefer, W. P.; Wing, R. M. *J. Am. Chem. Soc.* **1986**, *108*, 936.

(15) Chaudhuri, P.; Verani, C. N.; Bill, E.; Bothe, E.; Weyhermüller, T.; Wieghardt, K. *J. Am. Chem. Soc.* **2001**, *123*, 2213.

Chart 1. Ligands and Complexes

Ligands

Complexes

M[II]	$[M^{II}(L^{Bu\bullet})_2]$	$[M^{II}(L^{Bu\bullet})(L^{Bu})]^{1-}$	$[M^{II}(L^{Bu})_2]^{2-}$
Ni	**1**	**1a**	**1b**
Pd	**2**	**2a**	**2b**
Pt	**3**	**3a**	**3b**

$[Au^{III}(L^{Bu\bullet})(L^{Bu})]^0$ (**4**) $[Au^{III}(L^{Bu})_2]^{1-}$ (**4a**)

$[Cu^{III}(L^{Bu})_2]^{1-}$ (**5**)

density functional theoretical calculations on $[Cu^{III}(pds)_2]^-$ have clearly established the presence of a Cu^{III} (d[8], $S = 0$) ion (pds[2−] represents the ligand pyrazine-2,3-dithiolate(2−)).[16]

Also, the electronic structure of $[Au(L)_2]^-$ has been studied[17] by ab initio calculations, and it was shown that this species is best described as a Au^{III} (d[8], $S = 0$) species with two closed-shell benzene-1,2-dithiolate(2−) ligands. The one-electron oxidation yielding neutral $[Au(L)_2]^0$ was proposed to be predominantly ligand-centered yielding $[Au^{III}(L^{\bullet})(L)] \leftrightarrow [Au^{III}(L)(L^{\bullet})]$. In this work we have synthesized the square planar bis(3,5-di-*tert*-butylbenzene-1,2-dithiolato)metal complexes of palladium, platinum, and copper shown in Chart 1. Those of nickel[7] and gold[8] have been reported previously.

Experimental Section

The ligand 3,5-di-*tert*-butylbenzene-1,2-dithiol, $H_2[L^{Bu}]$, and the nickel complex $[Ni(L^{Bu\bullet})_2]$ (**1**) have been prepared as described in refs 6 and 7.

[N(n-Bu)₄][Ni(L^{Bu})(L$^{Bu\bullet}$)] (1a). To a solution of the ligand $H_2[L^{Bu}]$ (0.65 g; 2.6 mmol) in absolute ethanol (10 mL) was added a solution of potassium metal (240 mg) in absolute ethanol (5 mL) under an argon-blanketing atmosphere. To this solution was added solid $NiCl_2 \cdot 6H_2O$ (0.31 g; 1.3 mmol) and $[N(n-Bu)_4]Br$ (0.41 g, 1.3 mmol) at ambient temperature. The resulting reddish solution was stirred for 30 min in the presence of air whereupon a greenish residue precipitated which was collected by filtration. The crude material was recrystallized from a CH_2Cl_2/ethanol mixture (1:1 v:v) yielding shining green microcrystals of **1a** (0.78 g; 73%). Anal. Calcd for $C_{44}H_{76}S_4NNi$: C, 65.57; H, 9.50; N, 1.74. Found: C, 65.8; H, 9.4; N, 1.8. Electrospray mass spectrum (ESI) (CH_2Cl_2 solution): $m/z = 564.03$ (neg ion mode) $[Ni(L^{Bu})_2]^-$ and 242.3 $[N(n-Bu)_4]^+$ (pos ion mode).

[N(n-Bu)₄]₂[Ni(L^{Bu})₂] (1b). To a degassed solution of the ligand $H_2[L^{Bu}]$ (0.25 g; 1.0 mmol) and $[N(n-Bu)_4]Br$ (0.32 g; 1.0 mmol)

(16) Ribas, X.; Dias, J. C.; Morgado, J.; Wurst, K.; Molins, E.; Ruiz, E.; Almeida, M.; Veciana, J.; Rovira, C. *Chem.−Eur. J.* **2004**, *10*, 1691.

(17) Schiødt, N. C.; Sommer-Larsen, P.; Bjørnholm, T.; Folmer-Nielsen, M.; Larsen, J.; Bechgaard, K. *Inorg. Chem.* **1995**, *34*, 3688.

in absolute methanol (10 mL) was added NaOMe (0.24 g, 4 mmol), $NiCl_2 \cdot 6H_2O$ (0.12 g; 0.5 mmol), and an argon atmosphere (glovebox). The solution was stirred for ~12 h at ambient temperature during which time an extremely air-sensitive reddish-brown powder of **1b** precipitated. Yield: 0.29 g (54%). Anal. Calcd for $C_{60}H_{112}S_4N_2$-Ni: C, 68.74; H, 10.77; N, 2.67. Found: C, 68.9; H, 10.6; N, 2.5. ESI mass spectrum (CH_2Cl_2 solution): $m/z = 564.03$ $[Ni(L^{Bu})_2]^-$ (oxidized dianion) and 242.3 $[N(n-Bu)_4]^+$.

[Pd^{II}(L$^{Bu \bullet}$)$_2$] (2) and [Pt^{II}(L$^{Bu \bullet}$)$_2$] (3). These complexes have been generated electrochemically by one-electron oxidation at a controlled, fixed potential of +0.2 V vs Fc$^+$/Fc at ambient temperature of a CH_2Cl_2 solution (5 mL; 0.10 M $[N(n-Bu)_4]PF_6$) containing **2a** or **3a** in 1 mM concentration.

[N(*n*-Bu)$_4$][Pd^{II}(L^{Bu})(L$^{Bu \bullet}$)] (2a). To a solution of the ligand $H_2[L^{Bu}]$ (0.13 g; 0.5 mmol) in dimethylformamide (2 mL) was added dropwise a solution of $[N(n-Bu)_4]_2PdCl_6$ (0.20 g; 0.25 mmol) in CH_3CN (9 mL) under an Ar-blanketing atmosphere. After addition of 0.5 mL of ethanol the solution was heated to 40 °C for 30 min during which time the color of the solution changed from dark brown to light green. The solution was allowed to cool to 20 °C and was kept under a continuous flow of Ar gas for 3 h. Shining, light green microcrystals precipitated, which were collected by filtration. Yield: 0.12 g (54%). Anal. Calcd for $C_{44}H_{76}S_4NPd$: C, 61.85; H, 8.29; N, 1.64. Found: C, 62.0; H, 8.4; N, 1.6. ESI mass spectrum (pos and neg ion mode CH_2Cl_2 solution): $m/z = 610$ $[Pd(L^{Bu})_2]^-$ and 242.3 $[N(n-Bu)_4]^+$.

[PPh$_4$]$_2$[Pd^{II}(L)$_2$] (2b*). To an absolutely anaerobic solution of the ligand $H_2[L]$ (0.28 g; 2 mmol) and trimethylamine (0.4 mL) in dry methanol (30 mL) were added $PdCl_2$ (0.18 g; 1.0 mmol) and [PPh$_4$]Br (0.85 g; 2.0 mmol). The resulting solution was stirred at 20 °C for 12 h, after which time bright orange microcrystals had precipitated which were collected by filtration under an Ar-blanketing atmosphere. Recrystallization from CH_3CN yielded dark orange cubes suitable for X-ray diffraction. Anal. Calcd for $C_{60}H_{48}S_4P_2Pd$: C, 67.63; H, 5.26. Found: C, 67.6; H, 5.1. ESI mass spectrum (neg and pos ion mode; CH_2Cl_2 solution): $m/z = 386$ $[Pd(L)_2]^-$ (oxidized species) and 343.3 $[PPh_4]^+$.

[N(*n*-Bu)$_4$]$_2$[Pd(L^{Bu})$_2$] (2b). To a solution of the ligand $H_2[L^{Bu}]$ (0.25 g; 1.0 mmol), NaOMe (0.24 g, 4 mmol), and $[N(n-Bu)_4]Br$ (0.32 g; 1.0 mmol) in methanol (10 mL) was added $PdCl_2$ (0.88 g; 0.5 mmol) under strictly anaerobic conditions in a glovebox. The solution was stirred at 20 °C for 12 h, during which time an extremely air-sensitive reddish-brown powder precipitated. Yield: 0.30 g (54%). Anal. Calcd for $C_{60}H_{112}S_4N_2Pd$: C, 65.74; H, 10.30; N, 2.56. Found: C, 65.9; H, 10.4; N, 2.4. ESI mass spectrum (pos and neg ion mode; CH_2Cl_2 solution): $m/z = 610$ $[Pd(L^{Bu})_2]^-$ and 242.3 $[N(n-Bu)_4]^+$.

[N(*n*-Bu)$_4$][Pt^{II}(L^{Bu})(L$^{Bu \bullet}$)] (3a). This compound has been prepared as described above for **2a** by using $[N(n-Bu)_4]_2PtCl_6$ as starting material. Yield: 62%. Anal. Calcd for $C_{44}H_{76}S_4NPt$: C, 56.08; H, 8.14; N, 1.49. Found: C, 56.3; H, 8.3; N, 1.6. ESI mass spectrum (pos and neg ion mode; CH_2Cl_2 solution: $m/z = 700.1$ $[Pt(L^{Bu})_2]^-$ and 242.3 $[N(n-Bu)_4]^+$.

[N(*n*-Bu)$_4$]$_2$[Pt(L^{Bu})$_2$] (3b). To a solution of the ligand $H_2[L^{Bu}]$ (0.25 g; 1.0 mmol), NaOMe (0.24 g, 4 mmol), and $[N(n-Bu)_4]Br$ (0.32 g; 1.0 mmol) in methanol (10 mL) was added $PtCl_2$ (0.13 g; 0.5 mmol) under strictly anaerobic conditions (glovebox; N_2). The solution was stirred at 20 °C for 12 h, after which time an extremely air-sensitive red-brown powder had formed which was collected by filtration. Yield: 0.36 g (62%). Anal. Calcd for $C_{60}H_{112}S_4N_2Pt$: C, 60.82; H, 9.53; N, 2.36. Found: C, 61.0; H, 9.6; N, 2.3. ESI mass spectrum (pos and neg ion mode; CH_2Cl_2 solution): $m/z = 700.1$ $[Pt(L^{Bu})_2]^-$ (oxidized species) and 242.3 $[N(n-Bu)_4]^+$.

[Au^{III}(L^{Bu})(L$^{Bu \bullet}$)] (4) and [Au^{III}(L^{Bu})$_2$] [N(*n*-Bu)$_4$] (4a). These complexes have been synthesized as described in ref 8.

[N(*n*-Bu)$_4$][Cu^{III}(L^{Bu})$_2$] (5). Sodium metal (0.069 g; 3.0 mmol) was added to a solution of $[N(n-Bu)_4]Br$ (0.16 g; 0.5 mmol) and the ligand $H_2[L^{Bu}]$ (0.25 g; 1.0 mmol) in absolute ethanol (10 mL). A solution of $CuCl_2 \cdot 2H_2O$ (0.085 g; 0.5 mmol) in ethanol (8 mL) was added dropwise to the above solution at 20 °C. The resulting red solution was stirred for 0.5 h at 20 °C in the presence of air, during which time a green precipitate formed which was collected by filtration. The crude product was recrystallized from CH_2Cl_2 yielding light green microcrystals. Yield: 0.35 g (85%). Anal. Calcd for $C_{44}H_{76}S_4NCu$: C, 65.59; H, 9.45; N, 1.73. Found: C, 65.4; H, 9.4 N, 1.8. ESI mass spectrum (pos. and neg. ion mode; CH_2Cl_2 solution): $m/z = 567.2$ $[Cu(L^{Bu})_2]^-$ and 242.3 $[N(n-Bu)_4]^+$. By using $[As(CH_3)(C_6H_5)_3]Br$ instead of $[N(n-Bu)_4]Br$ in the above reaction, the complex $[As(CH_3)(C_6H_5)_3][Cu^{III}(L^{Bu})_2]$ (5′) was obtained. Single crystals suitable for X-ray crystallography were grown from a CH_2Cl_2/C_2H_5OH mixture (1:1 v:v).

X-ray Crystallographic Data Collection and Refinement of the Structures. A light violet single crystal of **2a**, an orange red crystal of **2b***, and a light green specimen of **5′** were coated with perfluoropolyether, picked up with a glass fiber, and mounted in the nitrogen cold stream of the diffractometer. Intensity data were collected on a Nonius Kappa-CCD diffractometer equipped with a Mo-target rotating-anode X-ray source and a graphite monochromator (Mo Kα, $\lambda = 0.710\ 73$ Å). Final cell constants were obtained from least-squares fits of all integrated reflections. Crystal faces of **2a** and **2b*** were determined, and the corresponding intensity data were corrected for absorption using the Gaussian-type routine embedded in XPREP.[18] The data set for **5′** was left uncorrected. Crystallographic data of the compounds are listed in Table 1. The Siemens ShelXTL[18] software package was used for solution and artwork of the structure, and ShelXL97[19] was used for the refinement. The structures were readily solved by direct and Patterson methods and subsequent difference Fourier techniques. All non-hydrogen atoms were refined anisotropically, and hydrogen atoms were placed at calculated positions and refined as riding atoms with isotropic displacement parameters. Compound **5′** crystallizes in space group $P1$. No additional symmetry was found, but crystals appeared to be racemically twinned. The *tert*-butyl groups bound to C(4) and C(24) were found to be disordered. Two split positions for each of the four carbon atoms were refined with occupancies in a 57:43 ratio. Chemically equal C−C distances were restrained to have similar values using the SADI Instruction of ShelXL, and equal anisotropic displacement parameters were refined for corresponding C atoms.

Physical Measurements. Electronic spectra of complexes and spectra of the spectroelectrochemical measurements were recorded on a Perkin-Elmer Lambda 9 spectrophotometer (range: 200−2000 nm). Cyclic voltammograms and coulometric measurements were performed with an EG&G potentiostat/galvanostat. X-band EPR spectra were recorded with a Bruker ESR 300 spectrometer. Infrared spectra were measured as KBr disks (or in CH_2Cl_2 solution; NaCl windows) on a Perkin-Elmer FFIR spectrophotometer 2000.

Calculations. All calculations in this work were performed with the electronic structure program ORCA.[20] All electron DFT-based geometry optimizations were carried out using the BP86 func-

(18) *ShelXTL V.5*; Siemens Analytical X-ray Instruments Inc.: Madison, WI, 1994.
(19) Sheldrick, G. M. *ShelXL97*; Universität Göttingen: Göttingen, Germany, 1997.

Table 1. Crystallographic Data for **2a**, **2b***, and **5′**

param	2a	2b*	5
chem formula	$C_{44}H_{76}NPdS_4$	$C_{60}H_{48}P_2PdS_4$	$C_{47}H_{58}AsCuS_4$
fw	853.70	1065.56	889.63
space group	$C2/c$, No. 15	$P2_1/n$, No. 14	$P1$, No. 1
a, Å	26.438(2)	11.0521(6)	8.3444(4)
b, Å	10.1521(8)	14.7262(8)	9.5921(4)
c, Å	18.098(2)	14.9977(8)	15.6799(9)
α, deg	90	90	83.80(1)
β, deg	102.79(1)	95.13(1)	83.23(1)
γ, deg	90	90	66.76(1)
V, Å	4737.0(7)	2431.2(2)	1142.6(1)
Z	4	2	1
T, K	200(2)	100(2)	100(2)
ρ_{calcd}, g cm^{-3}	1.197	1.456	1.293
reflcns collcd/$2\theta_{max}$	27 273/47.62	18 765/55.0	17 544/61.2
unique reflcns/$I > 2\sigma(I)$	3629/2931	5496/4305	10 758/9767
no. of params/restr	236/0	304/0	503/141
μ(Mo Kα), cm^{-1}	5.96	6.60	14.10
R1^a/goodness of fit^b	0.0363/1.040	0.0408/1.045	0.0471/1.021
wR2^c ($I < 2\sigma(I)$)	0.0647	0.0768	0.1112
resid density, e Å^{-3}	+0.26/−0.31	+0.49/−0.43	+1.37/0.59

^{a} Observation criterion: $I > 2\sigma(I)$. R1 $= \sum||F_o| - |F_c||/\sum|F_o|$. ^{b} GooF $= [\sum[w(F_o^2 - F_c^2)^2]/(n - p)]^{1/2}$. ^{c} wR2 $= [\sum[w(F_o^2 - F_c^2)^2]/\sum[w(F_o^2)^2]]^{1/2}$, where $w = 1/\sigma^2(F_o^2) + (aP)^2 + bP$ and $P = (F_o^2 + 2F_c^2)/3$.

tional.[21] Since this work is concerned with heavy transition metal complexes, scalar relativistic corrections were included using the second-order Douglas−Kroll−Hess (DKH2) method.[22] In the geometry optimizations the one-center approximation was used which eliminates DKH2 contributions to the analytic gradients. In the context of the zeroth-order regular approximation (ZORA),[23a] it was shown that the one-center approximation only introduces minor errors into the final geometries.[23] Large uncontracted Gaussian basis sets were used at the metal center which were derived from the well-tempered basis sets of Huzinaga.[24] For the remaining atoms the all-electron polarized triple-ξ (TZVP)[25a,b] Gaussian basis sets of the Ahlrichs group were used in an uncontracted form to allow for a distortion of the inner shell orbitals in the presence of the relativistic potential.

The property calculations at the optimized geometries were done with the B3LYP functional.[26] In this case the same basis sets were used but the scalar-relativistic ZORA method was used since in this formalism magnetic properties are more readily formulated.[27a] For the ZORA calculations, the method of van Wüllen[27b] is implemented in ORCA. Care was taken to ensure accurate numerical integration in the presence of steep basis functions. Details of the methods used to calculate the **g**-tensor and metal hyperfine couplings can be found in refs 28a,b. Although a

multicenter mean-spin−orbit coupling (SOC) operator has recently been implemented into ORCA,[28c] we have not used it here, due to the limitations of the underlying Breit−Pauli approach for heavier metals such as Pt. Instead, the effective nuclear charge model of Koseki was employed.[28d,e] However, since we have performed all-electron calculations using scalar relativistic corrections, the effective nuclear charges for Pd, Pt, and Au needed to be adjusted. From comparison between calculated SOC matrix elements with effective one-electron SOC constants the values $Z_{eff}(Pd) = 14.3$, $Z_{eff}(Pt) = 22.5$, and $Z_{eff}(Au) = 27.5$ were determined which lead to ζ_{nd} values of $\sim$1300 cm^{-1} (Pd), $\sim$3400 cm^{-1} (Pt), and $\sim$4500 cm^{-1} (Au), respectively. All other effective nuclear charges had their default values. TD-DFT calculations were carried out according to ref 28f.

Ab initio calculations of the optical spectra of the neutral [M(L)$_2$] complexes with M = Ni, Pd, and Pt were also undertaken with the ORCA program and utilized the recently developed spectroscopy oriented configuration interaction (SORCI) formalism.[13] Scalar-relativistic ZORA corrections were considered in the calculations. For the first row transition atoms, Wachters[29] basis sets were used at the metal center, contracted triple-ξ (TZVP)[25a,b] basis sets for the sulfurs, nitrogens, and oxygens, and SV(P) basis sets for the remaining atoms. For second row transition metals, the TZVP basis sets of Ahlrichs and May were used.[25c] For Pt we have recontracted the well-tempered basis set used in the geometry optimization in an atomic ZORA calculation as (34s24p19d13f) → [16s11p11d4f]. The selection threshold T_{sel} was 10^{-6} Eh, the prediagonalization threshold $T_{pre} = 10^{-6}$, and the natural orbital selection threshold $T_{nat} = 10^{-5}$. The calculations were started with spin-restricted orbitals from BP86 DFT calculations. The reference space was CAS(2,2) for the neutral complexes.

Natural population analysis (NPA)[30a−c] was done through an interface of ORCA to the Gennbo program version 5.0.[30d] Isocontour plots were done with the ChemBats3D program.[31]

(20) Neese, F. *Orca-an ab initio, DFT and semiempirical Electronic Structure Package*, version 2.4, revision 16; Max-Planck Institut für Bioanorganische Chemie: Mülheim, Germany, Nov 2004.

(21) (a) Becke, A. D. *J. Chem. Phys.* **1988**, *84*, 4524. (b) Perdew, J. P. *Phys. Rev. B* **1986**, *33*, 8522.

(22) Hess, B. A.; Marian, C. M. In *Computational Molecular Spectroscopy*; Jensen, P., Bunker, P. R., Eds.; John Wiley & Sons: New York, 2000; p 169 ff.

(23) (a) van Lenthe, E.; Snijders, J. G.; Baerends, E. J. *J. Chem. Phys.* **1996**, *105*, 6505. (b) van Lenthe J. H.; Faas, S.; Snijders J. G. *Chem. Phys. Lett.* **2000**, *328*, 107.

(24) (a) Huzinaga, S.; Miguel, B. *Chem. Phys. Lett.* **1990**, *175*, 289. (b) Huzinaga, S.; Klobukowski, M. *Chem. Phys. Lett.* **1993**, *212*, 260.

(25) (a) Schäfer, A.; Horn, H.; Ahlrichs, R. *J. Chem. Phys.* **1992**, *97*, 2571. (b) Schäfer, A.; Huber, C.; Ahlrichs, R. *J. Chem. Phys.* **1994**, *100*, 5289. (c) Ahlrichs, R.; May, K. *Phys. Chem. Chem. Phys.* **2000**, *2* 943−945.

(26) (a) Lee, C. Yang, W. Parr, R. G. *Phys. Rev. B* **1988**, *37*, 785. (b) Becke, A. D. J.*Chem. Phys.* **1993**, *98*, 5648.

(27) (a) van Lenthe E.; van der Avoird, A,; Wormer, P. E. S. *J. Chem. Phys.* **1998**, *108*, 4783. (b) van Wüllen, C. *J. Chem. Phys.* **1998**, *109*, 392.

(28) (a) Neese, F. *J. Chem. Phys.* **2001**, *115*, 11080. (b) Neese, F. *J. Chem. Phys.* **2003**, *118*, 3939. (c) Neese, F. *J. Chem. Phys.* **2005**, *122*, 034107. (d) Koseki, S.; Gordon, M. S.; Schmidt, M. W.; Matsunaga, N. *J. Phys. Chem.* **1995**, *99*, 12764. (e) Koseki, S.; Schmidt, M. W.; Gordon, M. S. *J. Phys. Chem. A* **1998**, *102*, 10430. (f) Neese, F.; Olbrich, G. *Chem. Phys. Lett.* **2002**, *362*, 170.

(29) Wachters, A. J. H. *J. Chem. Phys.* **1970**, *52*, 1033.

Table 2. Redox Potentials of $[M(L^{Bu})_2]^z$ ($z = 2-$, $1-$, 0) Complexes in CH_2Cl_2 Solution (0.10 M $[N(n\text{-}Bu)_4]PF_6$) at 20 °C

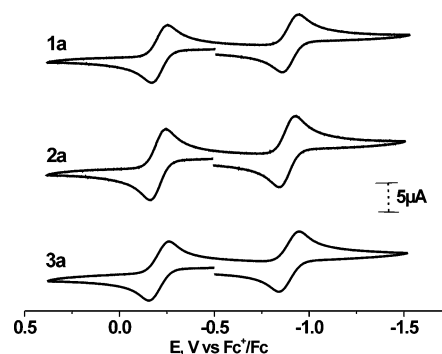| complex	$E^1_{1/2}$, V vs Fc$^+$/Fc	$E^2_{1/2}$, V vs Fc$^+$/Fc
1a	−0.23	−1.10
2a	−0.22	−0.92
3a	−0.27	−1.10
4a[a]	0.17	−2.18
5	0.17 (quasi reversible)	−1.44

[a] Reference 8.

Results

Synthesis. The reaction of disodium benzene-1,2-dithiolates, $Na_2[L^{Bu}]$ or $Na_2[L]$, with MCl_2 (M = Ni, Pd, Pt) in absolute ethanol under strictly anaerobic conditions in the ratio 2:1 yields the square planar, diamagnetic dianions $[M^{II}(L^{Bu})_2]^{2-}$ or $[M^{II}(L)_2]^{2-}$ (M = Ni, Pd, Pt) of which the bis(tetra-*n*-butylammonium) salts have been isolated: $[N(n\text{-}Bu)_4]_2[M(L^{Bu})_2]$ (M = Ni (**1b**), Pd (**2b**), Pt (**3b**)). These salts are very sensitive toward dioxygen both in the solid state and in solution. Thus, it has been possible to isolate $[N(n\text{-}Bu)_4][M(L^{Bu})(L^{Bu\bullet})]$ salts (M = Ni (**1a**), Pd (**2a**), Pt (**3a**)) from solutions of **1b**−**3b** exposed to air. These monoanions $[M(L^{Bu})(L^{Bu\bullet})]^-$ are also square planar but paramagnetic with an $S = 1/2$ ground state.

Further one-electron oxidation of **1a**, **2a**, or **3a** either chemically with 1 equiv of ferrocenium hexafluorophosphate or electrochemically via controlled potential coulometry (see below) affords light green, solutions of the square planar, diamagnetic, neutral complexes $[M^{II}(L^{Bu\bullet})_2]$ (M = Ni (**1**),[7] Pd (**2**), Pt (**3**)). These compounds possess an $S = 0$ ground state. Sellmann et al.[7] had prepared **1** by oxidation of **1a** with iodine in acetone solution as solid material and determined its crystal structure by X-ray crystallography.

Similarly, solid light-green $[N(n\text{-}Bu)_4][Cu^{III}(L^{Bu})_2]$ (**5**) has been synthesized by the reaction of $CuCl_2 \cdot 2H_2O$ with 2 equiv of $Na_2[L^{Bu}]$ in ethanol in the presence of air and addition of $[N(n\text{-}Bu)_4]Br$. This material is diamagnetic ($S = 0$). The salt $[As(CH_3)(C_6H_5)_3][Cu^{III}(L^{Bu})_2]$ (**5′**) has been obtained as single crystals suitable for X-ray crystallography. The synthesis and spectroscopic properties of $[Au^{III}(L^{Bu})(L^{Bu\bullet})]$ ($S = 1/2$) (**4**) and $[Au^{III}(L^{Bu})_2]^-$ ($S = 0$) (**4a**) have been described in ref 8.

Electro- and Spectroelectrochemistry. Cyclic voltammograms of complexes **1a**, **2a**, **3a**, and **5** have been recorded at 25 °C in CH_2Cl_2 solutions containing 0.10 M $[N(n\text{-}Bu)_4]$-PF_6 as supporting electrolyte and 0.1−1.0 mM complex by using a glassy carbon working electrode. Ferrocene was used as an internal standard; redox potentials are referenced versus the ferrocenium/ferrocene (Fc$^+$/Fc) couple. Table 2 summarizes the results.

Figure 1 shows the CVs of **1a**, **2a**, and **3a** recorded at a scan rate of 200 mV s^{-1} at 25 °C. Each compound displays two reversible one-electron transfer waves at nearly identical

(30) (a) Reed, A. E.; Weinhold, F. *J. Chem. Phys.* **1983**, *78*, 4066. (b) Reed, A. E.; Weinstock, R. B.; Weinhold, F. *J. Chem. Phys.* **1985**, *83*, 735. (c) Reed, A. E.; Curtiss, L. A.; Weinhold, F. *Chem. Rev.* **1988**, *88*, 899. (d). Glendening, E. D.; Badenhoop, J. K.; Reed, A. E.; Carpenter, J. E.; Bohmann, J. A.; Morales, C. M.; Weinhold F. *NBO 5.0*; Theoretical Chemistry Institute, University of Wisconsin: Madison, WI, 2001; http://www.chem.wisc.edu/~nbo5.
(31) *ChemBats3d*, version 6.0; CambridgeSoft.com, 2000.

Figure 1. Cyclic voltammograms of **1a** (top), **2a** (middle), and **3a** (bottom) in CH_2Cl_2 solution (0.10 M $[N(n\text{-}Bu)_4]PF_6$. Conditions: scan rate 200 mV s^{-1} at 25 °C (glassy carbon working electrode; ferrocene (Fc) internal standard).
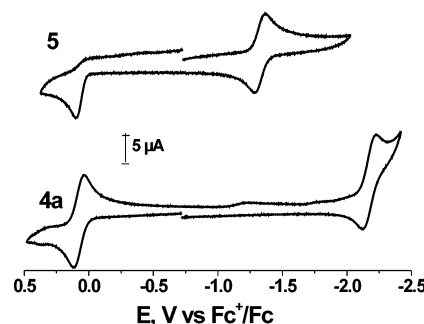
Figure 2. Cyclic voltammograms of **5** (top) and **4a** (bottom) in CH_2Cl_2 solution (0.10 M $[N(n\text{-}Bu)_4]PF_6$). Conditions are as in Figure 1.

redox potentials. Coulometric measurements established that each of the monoanions in **1a**, **2a**, and **3a**, $[M(L^{Bu})(L^{Bu\bullet})]^-$, undergoes a reversible one-electron oxidation and a reversible one-electron reduction. Thus, the three-membered electron-transfer series consisting of $[M^{II}(L^{Bu})_2]^{2-}$, $[M^{II}(L^{Bu})(L^{Bu\bullet})]^-$, and $[M^{II}(L^{Bu\bullet})_2]^0$ (M = Ni, Pd, Pt) is clearly established. Similar results have been reported for the series containing the unsubstituted benzene-1,2-dithiolate or its toluene-3,4-dithiolate analogues.[3]

The results in Figure 1 and Table 2 for **1a**, **2a**, and **3a** clearly show that the one-electron oxidation and the one-electron reduction must involve orbitals which display predominantly ligand character because the potentials $E^1_{1/2}$ and $E^2_{1/2}$ are nearly independent of the nature of the central metal ion Ni, Pd, or Pt.

In contrast, the CVs of complexes **4a** and **5** shown in Figure 2 display both a reversible (**4a**) and a quasi-reversible (**5**) one-electron oxidation at the same redox potential of +0.17 V for the $[M^{III}(L^{Bu\bullet})(L^{Bu})]^0/[M^{III}(L^{Bu})_2]^-$ couple, eq 1, but the corresponding one-electron reductions at −2.18 V for **4a**[8] and −1.44 V for **5** differ by 0.74 V indicating the metal-centered character of these reductions, eq 2.
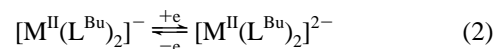
$$[M^{III}(L^{Bu})_2]^- \underset{+e}{\overset{-e}{\rightleftharpoons}} [M^{III}(L^{Bu})(L^{Bu\bullet})]^0 \qquad (1)$$

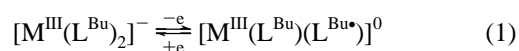$$[M^{II}(L^{Bu})_2]^- \underset{-e}{\overset{+e}{\rightleftharpoons}} [M^{II}(L^{Bu})_2]^{2-} \qquad (2)$$

Figure 3 displays the infrared spectra (KBr disks) of solid **1** and **1a,b** in the range 500−1500 cm^{-1}. It is quite remarkable that the tetra-*n*-butylammonium salts **1a,b** exhibit
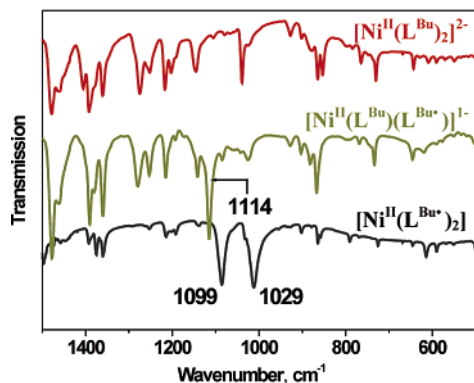
Figure 3. Infrared spectra of solid **1** (black), **1a** (green), and **1b** (red) in the range 500−1500 cm^{-1} (KBr disks). The spectra of the tetra-*n*-butylammonium salts of **1a,b** were recorded.

Table 3. ν(CdS•) Stretching Mode of Complexes

complex	ν(C=S•), cm^{-1}	complex	ν(C=S•), cm^{-1}
1	1099	**3a**	1109
1a	1114	**3b**	not obsd
1b	not obsd	**4**^{a}	1085
2	1082	**4a**^{a}	not obsd
2a	1102	**5**	not obsd
2b	not obsd	**6**	not obsd
3	1088		

different spectra: **1a** displays a frequency at 1114 cm^{-1}, which is absent in the corresponding spectrum of **1b**. In the spectrum of neutral **1** the former frequency is again observed at 1099 cm^{-1} (Table 3), whereas the band at 1029 cm^{-1} has only gained intensity in comparison with the spectra of **1a,b**. As we have shown previously for **4** and **4a**, the former displays this band at 1085 cm^{-1} and is absent in the spectrum of **4a**.[8] We have pointed out that this band is a marker for the presence of S,S-coordinated (L$^{Bu•}$)$^-$ radicals in square planar coordination compounds containing the 3,5-di-*tert*-butyl-benzene-1,2-dithiolato ligands.

To make a comparative study of the infrared spectra of **2**, **2a,b**, **3**, and **3a,b** we have generated the neutral and dianionic forms in CH$_2$Cl$_2$ solutions (0.10 M [N(n-Bu)$_4$]PF$_6$) by coulometry from **2a** and **3a**, respectively, and recorded their solution infrared spectra. These are displayed in Figure 4, and the ν(C=S•) frequencies are summarized in Table 3. It is immediately clear that **2**, **2a**, **3**, and **3a** exhibit ν(C=S•) bands but **2b** and **3b** do not. Thus, **2a** and **3a** may best be described as [M^{II}(L$^{Bu•}$)(L^{Bu})]$^-$ and **2** and **3** as [M^{II}(L$^{Bu•}$)$_2$] (M = Pd, Pt), whereas **2b** and **3b** are [M^{II}(L^{Bu})$_2$]$^{2-}$ (M = Pd, Pt) species.

Interestingly, the spectrum of the tetra-*n*-butylammonium salt of **5** does not display such a ν(C=S•) band. In this case also no π radical anions are present and the monoanion should be described as [Cu^{III}(L^{Bu})$_2$]$^-$.

The present IR results on [M(L^{Bu})$_2$]$^{n-}$, [M(L^{Bu})(L$^{Bu•}$)]$^{m-}$, and [M(L$^{Bu•}$)$_2$] complexes establish that the presence of one or two π radical anions enhances the intensity of the ν(C=S•) stretching mode to an extent where it is observed as a band of medium intensity in the infrared spectrum.

The electronic spectra of all complexes have been recorded in CH$_2$Cl$_2$ solutions in the range 300−1500 nm; the results are summarized in Table 4. Figure 5 exhibits the spectra of
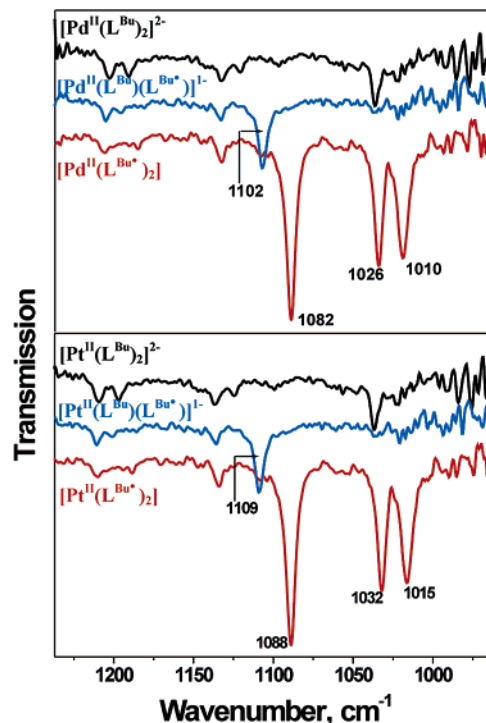
Figure 4. Infrared spectra of **2** (red), **2a** (blue), and **2b** (black) and **3** (red), **3a** (blue), and **3b** (black) in CH$_2$Cl$_2$ solution (0.10 M [N(n-Bu)$_4$]-PF$_6$) at −25 °C. Both neutral forms **2** and **3** and the dianions **2b** and **3b** were generated electrochemically.

Table 4. Electronic Spectra of Complexes in CH$_2$Cl$_2$ Solution

complex	T, °C	λ_{max}, nm (ϵ, 10^4 M^{-1} cm^{-1})
1^a	−25	309 (4.6), 348 (1.4), 378 (0.6), 600 (br, 0.2), 840 (3.0)
1a	20	303 (2.8), 389 (1.3), 698 (sh, 0.2), 890 (1.5)
1b^a	−25	310 (2.9), 398 (0.75)
2^a	−25	379 (1.2), 620 (0.8), 850 (5.0)
2a	20	340 (7.7), 408 (0.1), 894 (0.5), 1140 (2.5)
2b^a	−25	350 (0.9), 392 (0.6)
3^a	−25	320 (0.6), 390 (0.5), 802 (3.9)
3a	20	302 (1.5), 383 (0.3), 732 (0.2), 900 (1.9)
3b^a	−25	300 (1.5), 385 (0.25)
4^b	20	400 (0.6), 433 (0.34), 1023 (0.22), 1452 (2.7)
4a^b	20	380 (0.1), 415 (0.02), 618 (0.01)
5	20	343 (1.2), 398 (4.0)

^{a} Generated electrochemically at −25 °C. ^{b} Reference 8.

1a (top), **2a** (middle), and **3a** (bottom) together with their electrochemically generated one-electron-oxidized species **1**−**3** and their one-electron-reduced forms **1b**, **2b**, and **3b**. The assignment of the major absorption features follows in analogy to the assignments made in refs 9a,b and will be corroborated below though electronic structure calculations.

According to our interpretation, the most salient features of these spectra are the following: (a) The neutral species **1**−**3** display a very intense (>10^4 M^{-1} cm^{-1}) ligand-to-ligand charge-transfer band (LLCT) at 840, 850, and 802 nm, respectively. (b) Similarly, the monoanions **1a**, **2a**, and **3a** display an intense (>10^4 M^{-1} cm^{-1}) intervalence charge transfer band (IVCT) at 890, 1140, and 900 nm, respectively (the intensity of these IVCT bands of the monoanions is approximately half of that observed for the LLCT bands of the neutral species). (c) The dianions **1b**, **2b**, and **3b** do not absorb significantly (>10^2 M^{-1} cm^{-1}) above 400 nm. (d) All species exhibit an intense (>10^4 M^{-1} cm^{-1}) ligand-to-
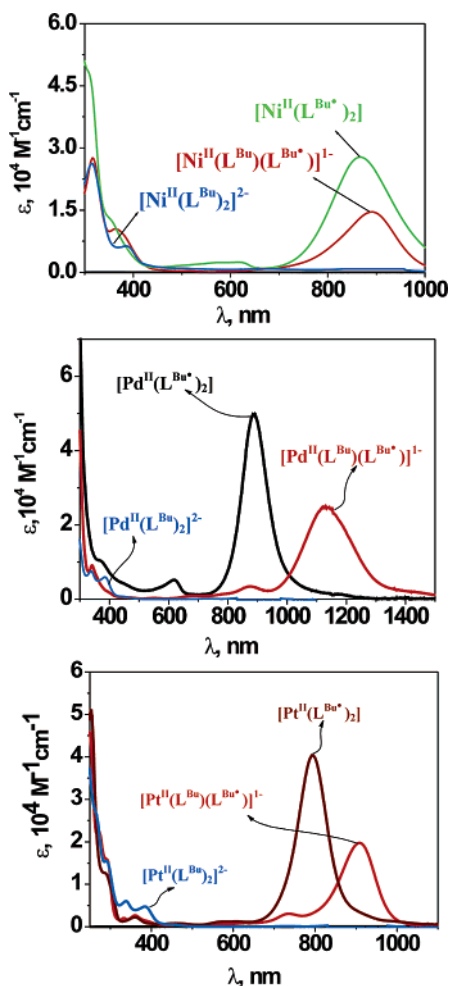
Figure 5. Electronic spectra of **1** (green), **1a** (red), and **1b** (blue) (top), of **2** (black), **2a** (red), and **2b** (blue) (middle), and of **3** (brown), **3a** (red), and **3b** (blue) in CH_2Cl_2 solutions (0.10 M [N(*n*-Bu)$_4$]PF$_6$) at −25 °C. The neutral forms **1**−**3** were generated electrochemically as have been the dianionic forms **1b**, **2b**, and **3b**.

metal charge-transfer bands (LMCT) and intraligand transitions <400 nm. It is noteworthy that [Au^{III}(L^{Bu})(L$^{Bu•}$)]^0 displays an IVCT band at 1452 nm ($\epsilon = 2.7 \times 10^4$ M^{-1} cm^{-1}) which is absent in [Au^{III}(L^{Bu})$_2$]$^{-}$.[8] The electronic spectrum of **5** in CH_2Cl_2 solution, on the other hand, does not display a prominent feature in the near-infrared which could be assigned to a LLCT or IVCT transition but instead shows an absorption band at 398 nm ($\epsilon = 4 \times 10^4$ M^{-1} cm^{-1}). On the basis of the calculations presented below, it will be argued that this transition is a LMCT band similar to that observed for the dianions **1b**, **2b**, and **3b**. In agreement with the results from IR spectroscopy, the monoanion is therefore a genuine Cu(III) species [Cu^{III}(L^{Bu})$_2$]$^{-}$.

Magnetic Properties and EPR Spectra. Complexes **1**−**3**, **4a**, and **5** are diamagnetic; they possess an $S = 0$ ground state as was judged from SQUID magnetometric and ^{1}H NMR measurements. The same is true for the species **1b**, **2b**, and **3b**, which are also diamagnetic. In contrast, complexes **1a**, **2a**, and **3a** are paramagnetic. The temperature-independent (50−300 K) effective magnetic moments are observed in the range 1.7−1.9 μ_B for **1a**, **2a**, and **3a** indicative of an $S = \frac{1}{2}$ ground state, respectively.
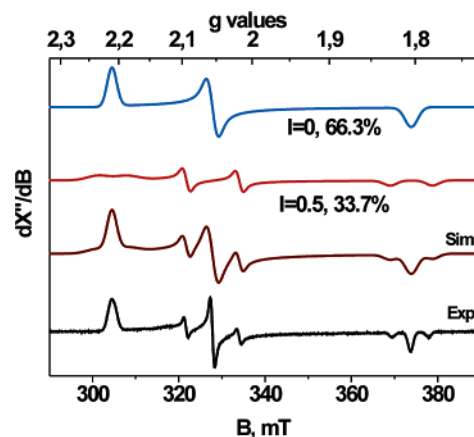

Figure 6. X-band EPR spectrum of **3a** in CH_2Cl_2 solution at 10 K. Conditions: frequency, 9.6355 GHz; modulation, 10 G; power, 504 W.

The X-band rhombic EPR spectrum of (AsPh$_4$)[Ni^{II}(L^{Bu})-(L$^{Bu•}$)] in CHCl$_3$/DMF solution has been reported:[7] $g_1 = 2.18$; $g_2 = 2.04$; $g_3 = 2.01$. By using a ^{61}Ni-enriched sample, hyperfine coupling with the ^{61}Ni ($I = \frac{3}{2}$) nucleus was observed: $A_1(^{61}$Ni$) = 131(15)$, $A_2(^{61}$Ni$) < 17$, and $A_3(^{61}$Ni$) = 57(10)$ mT. This has been interpreted[7] as a strong indication for "considerable metal contribution to the SOMO". The electronic structure calculations described below provide metal contributions to the SOMO on the order of 30−35% depending on the method of population analysis. Similar values have been reported for (NR$_4$)[Ni(S$_2$C$_2$(CN)$_2$)$_2$][32] and (NR$_4$)[Ni(xylene-1,2-dithiolate)$_2$].[33] The spectrum of [Ni(L)$_2$]$^{-}$ is also very similar.[2−5]

The X-band EPR spectrum of **3a** in CH_2Cl_2 solution at 10 K is shown in Figure 6. A rhombic signal is observed: $g = 2.21$, 2.06, and 1.80. Hyperfine coupling to the ^{195}Pt ($I = \frac{3}{2}$; 33% abundance) with $A_{xx} = 320$ MHz, $A_{yy} = 278$ MHz, and $A_{zz} = 227$ MHz is recorded indicating significant metal spin density to be present.

In contrast, the corresponding spectrum for **2a** at 10 K does not display ^{105}Pd ($I = \frac{5}{2}$; 25% abundance) hyperfine coupling. An isotropic signal at $g_{iso} = 2.02$ is observed. It is noted that the EPR spectrum of [Au^{III}(L$^{Bu•}$)(L^{Bu})] (**4**) also does not display hyperfine coupling to ^{197}Au ($I = \frac{3}{2}$, 100% natural abundance).[8] However, before the conclusion that the metal spin density must be highest for **3a**, it should be recalled that the nuclear g-value of ^{195}Pt ($g_N = 1.219$) is roughly 5 times larger than that of ^{105}Pd ($g_N = -0.256$) and 12 times larger than that of ^{197}Au ($g_N = 0.097$). Thus, the hyperfine coupling constants (HFCs) of the central Pd might have been detected if the metal spin density were comparable to the Pt case whereas in the Au case the metal HFC splitting is likely to buried within the line width of the experiment.

X-ray Crystallography. Sellmann et al.[7] reported the crystal structures of [Ni^{II}(L$^{Bu•}$)$_2$] (**1**), [AsPh$_4$][Ni^{II}(L$^{Bu•}$)(L^{Bu})] (**1a**), and [AsPh$_4$]$_2$[Ni^{II}(L^{Bu})$_2$]·2Et$_2$O (**1b**). The results are summarized in Figure 7. The structures determined at 293 K are of good quality. The experimental errors of the C−C

(32) Maki, A. H.; Edelstein, M.; Davison, A.; Holm, R. H. *J. Am. Chem. Soc.* **1964**, *86*, 4580.
(33) Kirmse, R.; Stach, J.; Dietzsch, W.; Steinecke, G.; Hoyer, E. *Inorg. Chem.* **1980**, *19*, 2679.
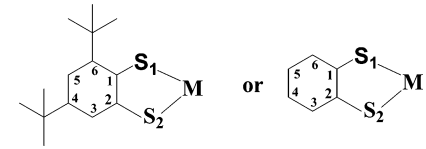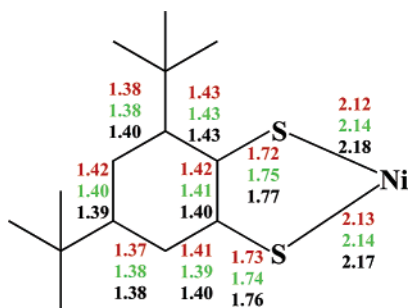
Figure 7. Selected average bond distances (Å) for square planar complexes [Ni(L^{Bu})$_2$] (red), [AsPh$_4$][Ni(L^{Bu})$_2$] (green), and [AsPh4]$_2$[Ni(L^{Bu})$_2$] (black) from ref 7. The average error for C−C and C−S bond distances is ±0.01 Å (3σ).

and C−S bond distances are of the order ±0.01 Å (≡3σ). Therefore, we wish to argue that the observed decrease of the average C−S bond length on going from **1b** (average 1.765 Å) to **1a** (average 1.745 Å) and to **1** (average 1.725 Å) reflects a real ligand-centered stepwise oxidation of two closed-shell aromatic dianions (L^{Bu})$^{2-}$ in **1b** to one such ligand and an additional π radical monoanion (L$^{Bu•}$)$^-$ in **1a** to *two* such radicals in the neutral species **1**. The oxidation state of the central nickel ion remains +II (d^8, S_{Ni} = 0) throughout the electron-transfer series. In particular, diamagnetic square planar **1** cannot contain a Ni(IV) (d^6) ion and two (L^{Bu})$^{2-}$ ligands since an S = 1 ground state as is observed for isoelectronic [Co^{III}(L^{Bu})$_2$]$^-$ [34] would prevail according to simple ligand field considerations. The six C−C bonds of the six-membered ligand rings are nearly equidistant in **1b** (average 1.40 Å) but display weak quinoid-like distortions in **1a** and more pronounced so in **1**. This is excellent evidence that the HOMO in **1b** possesses ligand character with little metal d-orbital contributions.

Interestingly, in similar complexes containing the unsubstituted benzene-1,2-dithiolate ligands as in [N(CH$_3$)$_4$]$_2$[Ni(L)$_2$] the average C−S bond at 1.762(8) Å is long and the six C−C distances are within experimental error equidistant (average 1.40 Å).[35] In contrast, in two structure determinations of salts containing the monoanion [Ni(L)$_2$]$^-$ the C−S bonds are always shorter at average 1.74 Å and the six C−C bonds display two alternating shorter ones and four longer ones (quinoid-like distortion).[36] Similar results have been reported for the monoanion [Ni(L$^{Me•}$)(L^{Me})]$^-$.[37]

In this work we have determined the structures of [N(*n*-Bu)$_4$][Pd^{II}(L$^{Bu•}$)(L^{Bu})] (**2a**), [PPh$_4$]$_2$[Pd^{II}(L)$_2$] (**2b***), and [AsPh$_4$]-[Cu^{III}(L^{Bu})$_2$] (**5′**) at 100 K by X-ray crystallography. Table 5 summarizes important bond lengths; Figure 8 shows the structures of the monoanion in crystals of **2a** (top), the

(34) Ray, K.; Begum, A.; Weyhermüller, T.; Piligkos, S.; van Slagaren, J.; Neese, F.; Wieghardt, K. *J. Am. Chem. Soc.* **2005**, *127*, 4403−4415.
(35) Sellmann, D.; Fünfgelder, S.; Knoch, F.; Moll, M. *Z. Naturforsch.* **1991**, *46b*, 1601.
(36) Mahadevan, C.; Seshasayee, M.; Kuppusamy, P.; Manoharam, P. T. *J. Crystallogr. Spectrosc. Res.* **1985**, *15*, 305.
(37) (a) Ochocki, J.; Chaudhuri, P.; Driessen, W. L.; de Graaf, R. A. G.; Hulsbergen, F. B.; Reedijk, J. *Inorg. Chim. Acta* **1990**, *167*, 15. (b) Kamenicek, J.; Valach, F.; Kratochvil, B.; Zak, Z. *Pol. J. Chem.* **2002**, *76*, 483. (c) Robertson, N.; Parsons, S.; Awaga, K.; Fujita, W. *Cryst. Eng. Commun.* **2000**, 22.
(38) Cocker, T. M.; Bachman, R. E. *Inorg. Chem.* **2001**, *40*, 1550.
(39) Connick, W. B.; Gray, H. B. *J. Am. Chem. Soc.* **1997**, *119*, 11620.

Table 5. Bond Distances (Å) in the Anions of **2a**, **2b***, and **5′**

	2a	**2b***	**5**	
C1−S1	1.751(3)	1.758(3)	1.769(4)	1.770(4)
C2−S2	1.750(3)	1.764(3)	1.751(4)	1.767(5)
C1−C2	1.404(4)	1.400(4)	1.398(6)	1.394(6)
C2−C3	1.402(4)	1.406(4)	1.386(6)	1.415(5)
C3−C4	1.375(4)	1.382(4)	1.382(7)	1.366(8)
C4−C5	1.400(4)	1.395(4)	1.389(7)	1.405(8)
C5−C6	1.389(4)	1.385(4)	1.404(7)	1.404(5)
C1−C6	1.435(4)	1.404(4)	1.409(6)	1.419(6)
M−S1	2.2560(8)	2.3009(7)	2.170(1)	2.163(1)
M−S2	2.2633(8)	2.3087(7)	2.160(1)	2.173(1)

dianion in **2b*** (middle), and the monoanion in **5′** (bottom). All three species possess a planar MS$_4$ polyhedron. The tertiary butyl groups in **2a** and **5′** are in a trans-position relative to each other.

As expected, the C−S bonds in the dianion of **2b*** are long at average 1.76 ± 0.01 Å and the six C−C bonds are equidistant at 1.395 ± 0.01 Å. Therefore, the closed-shell, dianionic form of the ligand, (L)$^{2-}$, is coordinated to a Pd(II) ion (d^8, S = 0) as in square planar [(bpy)Pd^{II}(L)]^0 [38] and [(bpy)Pt^{II}(L)]^0.[39]

In the monoanion of **2a** the C−S bonds are slightly shorter at average 1.75 ± 0.01 Å and the six C−C bonds display
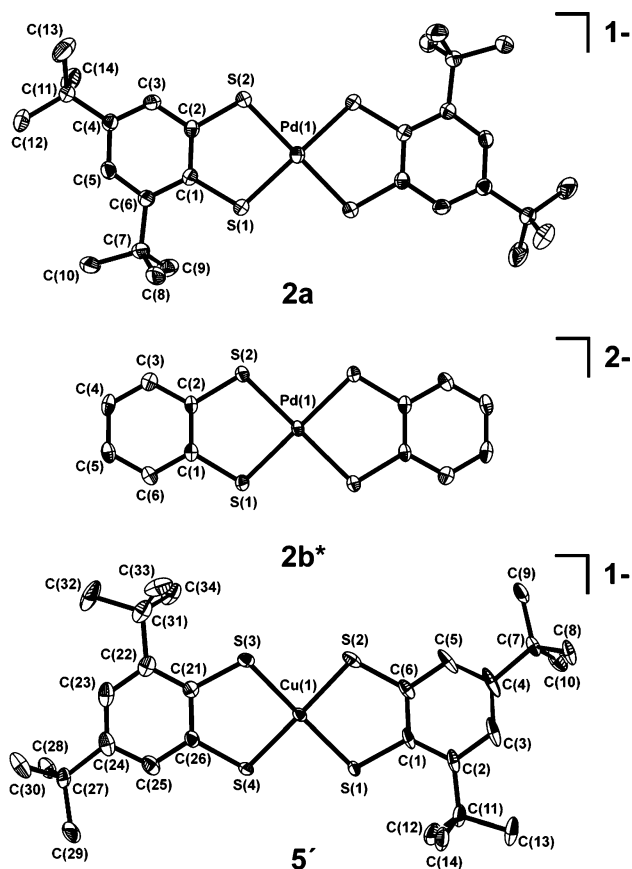

Figure 8. Structures of the monoanions in crystals of **2a** (top) and **5′** (bottom) and of the dianion in crystals of **2b***.

signs of a quinoid-like distortion. The two alternating C−C bonds C5−C6 at 1.389(4) Å and C3−C4 at 1.375(4) Å are shorter than the other four C−C bonds at average 1.41 ± 0.01 Å. The structure is very similar to that of [Ni(L$^{Bu•}$)(L^{Bu})]$^−$ [7] and is in accord with the notion that one-electron oxidation from the dianion to the corresponding monoanion (**1b** → **1a**; **2b** → **2a**; **3b** → **3a**) is a predominantly ligand-centered process.

The structure of the monoanion in crystals of **5′** on the other hand clearly shows that both ligands are in the closed-shell dianionic form (L^{Bu})$^{2−}$ rendering the central copper ion trivalent (Cu^{III}; d^8, $S = 0$). The average C−S bond length is long at 1.764 ± 0.01 Å, and the C−C distances do not show a quinoid-like distortion. This interpretation is in contrast to Sawyer et al.,[14] who reported a crystal structure of [N(*n*-Bu)$_4$][Cu(L^{Me})$_2$] which is of rather low quality with an error of ±0.1 Å for the C−S bond. These authors concluded from electrochemical results that the monoanion possesses a [Cu^{II}(L$^{Me•}$)(L^{Me})]$^−$ electronic structure. Two other structure determinations of [PPh$_4$][Cu(L)$_2$] and [PPh$_4$][Cu(L^{Me})$_2$] also have too large errors of ∼0.02 and 0.03 Å, respectively, for the C−S bond distances to determine unambiguously the oxidation level of the ligands.[40]

It is instructive to study the electronic structure of the uncoordinated ligand (L)$^{2−}$ and its planar dimer {(L)$_2$}$^{4−}$ first. The MO diagrams obtained from BP86 calculations are shown in Figure 9: the resulting MO's may be divided into out-of-plane (π, a$_2$, and b$_2$) and in-plane (σ, a$_1$, and b$_1$) orbitals. The redox-active MO is 2b$_2$, which is the HOMO for (L)$^{2−}$ and the SOMO for (L$^•$)$^−$. The 2b$_2$ MO is bonding between C$_4$ and C$_5$ but antibonding between C$_3$ and C$_4$ and C$_5$ and C$_6$ and also between the sulfur atoms and the adjacent carbon atoms C$_1$ and C$_6$, respectively. Thus, upon oxidation of the aromatic closed-shell dianion (L)$^{2−}$ to the semiquinon-ate form (L$^•$)$^−$ the C$_4$−C$_5$ bond expands slightly whereas the C$_3$−C$_4$ and C$_5$−C$_6$ and both C−S bonds shrink. The effect on the six-membered ring is small and inside the normal experimental error limit of a single-crystal X-ray structure determination, where an error of ±0.01 Å is considered to be normal. In contrast, the C−S bond distance changes are outside the experimental error limits. The calculated spin density of the H(L$^•$) radical in Figure 9 shows a large spin density at the deprotonated sulfur atom and limited delocalization of spin density on the six-membered phenyl ring. These results are in stark contrast to genuine oxygen-containing semiquinonates where delocalization of spin density onto the ring is much more pronounced.[41]

Calculations. 1. Ligands. Due to the localization of spin density at the sulfur atom the two-electron-oxidized form of (L)$^{2−}$ is calculated to be unstable against intramolecular disulfide bond formation. The calculated structure of L is shown in Figure 9 (bottom).

For the ligand dimer {(L)$_2$}$^{4−}$, the positive and negative combinations of the HOMO (2b$_2$) of two L$^{2−}$ give rise to the 1b$_{1u}$ and 1b$_{2g}$ orbitals (Figure 9), respectively. Due to the

(40) Mao-Chun, H.; Zhi-Ying, H.; Xin-Jiaw, L.; Ling-Hong, W.; Ham-Qin, L. *J. Struct. Chem.* **1991**, *10*, 237.
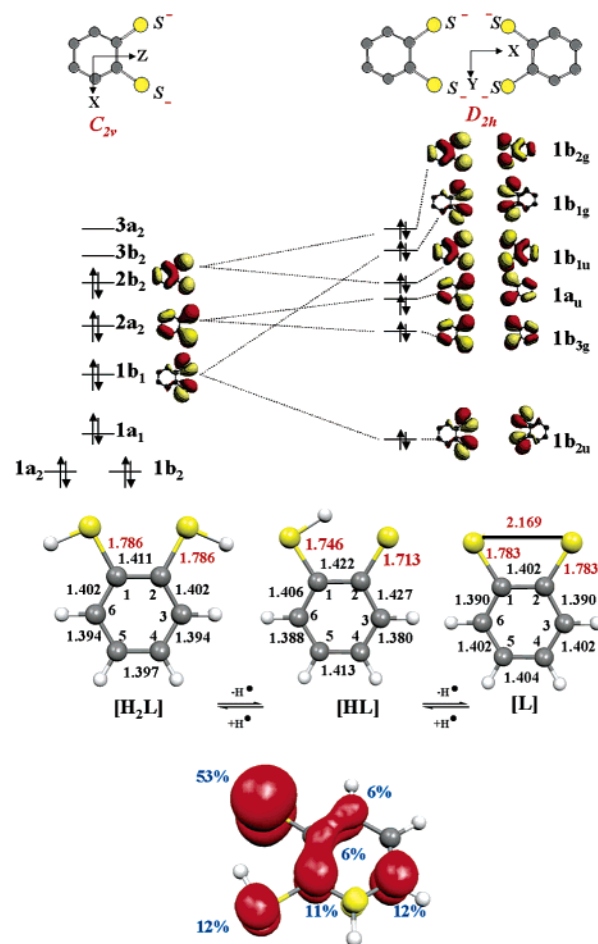
Figure 9. Top: MO diagram for benzene-1,2-dithiolate(2−) and its hypothetical planar dimer. Bottom: Bond distances (Å) from a geometry optimization (BP86, DFT, TZVP basis for sulfur atoms and SV(P) for the remaining atoms) on benzene-1,2-dithiol (H2L) and its deprotonated one-electron oxidized form (HL) and the fully deprotonated two-electron-oxidized form (L). The spin density distribution of the radical HL ($S = 1/2$) is shown below.
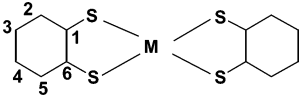
their respective symmetry only the 1b$_{2g}$ orbital can undergo a symmetry-allowed π interaction with a d$_{xz}$ orbital of a central transition metal ion. The extent of this mixing is of course dependent on the relative energies of the interacting orbitals. Similarly, the symmetric and antisymmetric combinations of the 2a$_2$ MOs give rise to the 1a$_u$ and 1b$_{3g}$ MOs where again only the 1b$_{3g}$ can π- interact with the d$_{yz}$ metal orbital. Finally, the antisymmetric combination of the 1b$_1$ MOs gives rise to a 1b$_{1g}$ orbital which can interact with the d$_{xy}$ metal orbital.

2. [M(L)(L$^•$)]^z Species with $S = {}^1/_2$ Ground State (M = Ni, Pd, Pt, $z = 1−$; Au, $z = 0$). (a) Geometries. As shown in Table 6 the optimized calculated structures of paramagnetic complexes [M(L)(L$^•$)]^z (M = Ni^{II}, Pd^{II}, Pt^{II}, $z = 1−$; Au^{III}, $z = 0$) are in excellent agreement with the experimental findings. The slight overestimation of the M−S bond distances is typical for present day DFT functionals. However, the metrical parameters for the dithiolate ligands are

(41) (a) Pierpont, C. G.; Lange, C. W. *Prog. Inorg. Chem.* **1994**, *41*, 331.
(b) Pierpont, C. G.; Buchanan, R. M. *Coord. Chem. Rev.* **1981**, *38*, 45.

Table 6. Experimental and Calculated (in Parentheses) Metrical Parameters for the Complexes in Å Obtained from Scalar Relativistic DKH2-BP86DFT Methods Using Large Uncontracted Gaussian Bases at the Metal Center and Uncontracted All Electron Polarized Triple-ξ (TZVP) Gaussian Bases for the Remaining Atoms

complex	M−S	C−S	C1−C2	C2−C3	C3−C4	C4−C5	C5−C6	C1−C6
[Ni(L)$_2$]$^{2-}$ ^{a}	2.173 (2.210)	1.762 (1.770)	1.426 (1.407)	1.398 (1.399)	1.390 (1.402)	1.383 (1.399)	1.402 (1.407)	1.401 (1.405)
[Ni(L)$_2$]$^{-}$ ^{a}	2.146 (2.181)	1.747 (1.763)	1.425 (1.407)	1.387 (1.390)	1.412 (1.405)	1.367 (1.390)	1.391 (1.407)	1.407 (1.413)
[Ni(L)$_2$]^{0} ^{a}	2.126 (2.158)	1.727 (1.744)	1.429 (1.412)	1.375 (1.382)	1.422 (1.412)	1.373 (1.382)	1.409 (1.412)	1.419 (1.424)
[Pd(L)$_2$]$^{2-}$	2.301 (2.358)	1.761 (1.773)	1.419 (1.408)	1.385 (1.397)	1.395 (1.401)	1.382 (1.397)	1.406 (1.408)	1.400 (1.403)
[Pd(L)$_2$]$^{-}$	2.263 (2.325)	1.751 (1.763)	1.435 (1.410)	1.389 (1.388)	1.400 (1.405)	1.375 (1.388)	1.402 (1.410)	1.404 (1.417)
[Pd(L)$_2$]^{0}	(2.300)	(1.744)	(1.414)	(1.381)	(1.412)	(1.381)	(1.414)	(1.421)
[Pt(L)$_2$]$^{2-}$	(2.318)	(1.770)	(1.408)	(1.397)	(1.402)	(1.397)	(1.408)	(1.405)
[Pt(L)$_2$]$^{-}$	(2.288)	(1.756)	(1.408)	(1.389)	(1.406)	(1.388)	(1.408)	(1.416)
[Pt(L)$_2$]^{0}	(2.261)	(1.739)	(1.411)	(1.381)	(1.412)	(1.381)	(1.411)	(1.419)
[Cu(L)$_2$]$^{-}$ ^{a}	2.168 (2.217)	1.768 (1.774)	1.419 (1.408)	1.404 (1.398)	1.405 (1.402)	1.366 (1.390)	1.415 (1.405)	1.394 (1.402)
[Au(L)$_2$]$^{-}$	2.310 (2.338)	1.764 (1.776)	1.397 (1.404)	1.386 (1.393)	1.392 (1.400)	1.382 (1.393)	1.402 (1.404)	1.397 (1.4 06)
[Au(L)$_2$]^{0}	2.300 (2.317)	1.735 (1.758)	1.402 (1.408)	1.374 (1.385)	1.415 (1.406)	1.384 (1.385)	1.420 (1.408)	1.406 (1.411)

^{a} Experimental values for complexes containing 3,5-di-*tert*-butyl-1,2-benzenedithiolate ligand.

very accurately reproduced by the calculations with the typical error in computed bond lengths not exceeding ∼0.02 Å.

The calculated average C−S bond length of 1.76 Å corresponds to the arithmetic average of calculated C−S bond distances at 1.79 Å for complexes containing only closed-shell (L)$^{2-}$ dianions and at 1.73 Å for species containing only (L$^•$)$^−$ radicals. Thus, as expected, the complexes behave like class III delocalized ligand mixed-valent systems [M(L$^•$)(L)]^z ↔ [M(L)(L$^•$)]^z in these calculations.

(b) Bonding. For the MO description of these paramagnetic complexes within the D_{2h} point group, we choose the z axis to be along the normal of the complex; the x axis is then along the long axis of the complex and the y axis along the short axis as shown in Figure 10. The qualitative bonding scheme derived from the spin-unrestricted B3LYP DFT calculation on the [Au^{III}(L)(L$^•$)]^0 species is also shown where
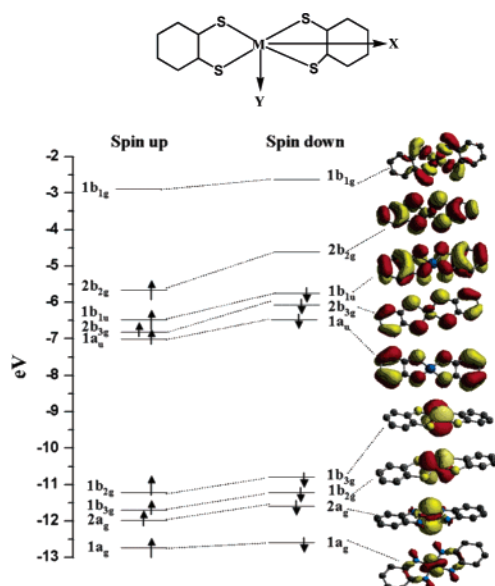

Figure 10. Kohn−Sham MOs and energy scheme for [Au(L)(L$^•$)]^0 from a spin-unrestricted ZORA-B3LYP DFT calculation.

the spin up and the spin down MOs are plotted in order of increasing energy. Since this bonding scheme does not change qualitatively for all [M(L)(L$^•$)]^z species under consideration here, it is equally applicable for the Ni, Pd, and Pt counterparts. The composition of important MOs is summarized in Table 7.

The ground-state electronic configuration of the [M(L$^•$)-(L)]^z species is predicted to be

$$(1a_g)^2(2a_g)^2(1b_{3g})^2(1b_{2g})^2(1a_u)^2(2b_{3g})^2(1b_{1u})^2(2b_{2g})^1(1b_{1g})^0$$

The ground state $^2B_{2g}$ is in agreement with earlier results from extended Hückel calculations on the [Ni(L$^•$)(L)]$^−$ complex.[10−12] The same ground state has been proposed for [M(L)(L$^•$)]$^−$ (M = Ni, Pd, Pt) complexes from an analysis of their EPR spectra.[2−5]

The bonding scheme in Figure 10 reveals that in general four metal d orbitals are lower in energy as compared to the ligand-based 1b$_{2g}$ and 1b$_{3g}$ orbitals shown in Figure 9 which undergo symmetry-allowed π interactions with metal d orbitals. This is consistent with recent calculations for the [Ni^{II}(S$_2$C$_2$Me$_2$)$_2$]$^−$ complex.[42] In these and our present calculations four doubly occupied orbitals, namely 1a$_g$(d$_{x^2-y^2}$), 2a$_g$(d$_{z^2}$), 1b$_{3g}$(d$_{yz}$), and 1b$_{2g}$(d$_{xz}$) are predominantly of metal-d character and, hence, the physical oxidation state of the metals is best represented as d^8 M^{II} (Ni, Pd, Pt) and Au^{III} ions.

The LUMO of these complexes is the antibonding combination of the metal d$_{xy}$ and the ligand 1b$_{1g}$ fragment orbitals. The overlap between these two orbitals is favorable and provides an efficient pathway for ligand-to-metal σ electron donation. The SOMO features mainly the π* 2b$_{2g}$ MO of the ligand which mixes with the metal d$_{xz}$ orbital. This interaction accounts for metal-to-ligand π electron donation in these paramagnetic complexes.

(c) Population Analysis. Table 8 summarizes the charge and spin populations at the respective metal ion resulting

(42) Szilagyi, R. K.; Lim, B. S.; Glaser, T.; Holm, R. H.; Hedman, B.; Hodgson, K. O.; Solomon, E. I. *J. Am. Chem. Soc.* **2003**, *125*, 9158.

Table 7. Composition of Selected Molecular Orbitals of $[M(L)_2]^z$ Complexes (%) As Obtained from the Scalar Relativistic ZORA-B3LYP DFT Calculations Using Large Uncontrated Gaussian Bases at the Metal and Uncontracted All Electron Polarized Triple-ξ (TZVP) Gaussian Bases for the Remaining Atoms

complex	MO	$M(nd_{yz})$	$M(nd_{xz})$	$M(nd_{xy})$	$S(3p_z)$	$S(3p_{x,y})$	$C(2p_z)$	$C(2p_{x,y})$
$[Ni(L)_2]^{2-}$	$2b_{3g}$	71			17		8	
	$2b_{2g}$		52		36		10	
	$1b_{1g}$			50		40		2
$[Ni(L)_2]^-$	$2b_{3g}$	55			30		10	
	$2b_{2g}$		34		48		14	
	$1b_{1g}$			46		43		5
$[Ni(L)_2]^0$	$2b_{3g}$	49			34		12	
	$2b_{2g}$		26		51		16	
	$1b_{1g}$			43		48		3
$[Pd(L)_2]^{2-}$	$2b_{3g}$	44			37		18	
	$2b_{2g}$		29		52		17	
	$1b_{1g}$			41		46		3
$[Pd(L)_2]^-$	$2b_{3g}$	33			44		19	
	$2b_{2g}$		21		56		21	
	$1b_{1g}$			40		48		3
$[Pd(L)_2]^0$	$2b_{3g}$	28			43		23	
	$2b_{2g}$		16		56		25	
	$1b_{1g}$			39		48		4
$[Pt(L)_2]^{2-}$	$2b_{3g}$	42			36		20	
	$2b_{2g}$		30		52		17	
	$1b_{1g}$			39		38		1
$[Pt(L)_2]^-$	$2b_{3g}$	33			44		19	
	$2b_{2g}$		24		56		18	
	$1b_{1g}$			41		42		2
$[Pt(L)_2]^0$	$2b_{3g}$	29			44		23	
	$2b_{2g}$		20		56		22	
	$1b_{1g}$			40		43		2
$[Cu(L)_2]^-$	$2b_{3g}$	17			53		30	
	$2b_{2g}$		11		58		27	
	$1b_{1g}$			33		58		4
$[Au(L)_2]^-$	$2b_{3g}$	11			58		30	
	$2b_{2g}$		9		64		26	
	$1b_{1g}$			33		55		5
$[Au(L)_2]^0$	$2b_{3g}$	9			51		38	
	$2b_{2g}$		8		61		30	
	$1b_{1g}$			33		55		5

Table 8. Comparison of the Charge and Spin Populations at the Metal Ion Resulting from a Natural Population Analysis of the One-Electron Density of the Ground State Obtained from Scalar Relativistic ZORA-B3LYP DFT Calculations[a]

complex	nd electrons	$(n+1)s$ electrons	nd spin	metal oxidn state
$[Ni(L)_2]^{2-}$	9.13	0.51	0.00	Ni^{II}
$[Ni(L)_2]^-$	9.01	0.53	0.31	Ni^{II}
$[Ni(L)_2]^0$	8.99	0.54	0.00	Ni^{II}
$[Pd(L)_2]^{2-}$	9.24	0.43	0.00	Pd^{II}
$[Pd(L)_2]^-$	9.16	0.47	0.16	Pd^{II}
$[Pd(L)_2]^0$	9.08	0.48	0.00	Pd^{II}
$[Pt(L)_2]^{2-}$	9.07	0.74	0.00	Pt^{II}
$[Pt(L)_2]^-$	8.97	0.76	0.21	Pt^{II}
$[Pt(L)_2]^0$	8.92	0.78	0.00	Pt^{II}
$[Cu(L)_2]^-$	8.92	0.49	0.00	Cu^{III}
$[Au(L)_2]^-$	8.99	0.63	0.00	Au^{III}
$[Au(L)_2]^0$	8.90	0.65	0.05	Au^{III}

[a] Spin restricted calculations are reported for the neutral $[M(L)_2]^0$ species with M = Ni, Pd, and Pt.

from a natural population analysis[30a−c] of the one-electron density of the ground state obtained from scalar reletavistic ZORA-B3LYP DFT calculations. The calculated nd populations for the complexes $[M(L^\bullet)(L)]^-$ (M = Ni, Pd, Pt) and $[Au(L^\bullet)(L)]^0$ are consistent with the nd^8 valence electron configuration. The charge excess over the formal nd^8 configuration arises from the population of the otherwise unpopulated nd_{xy} orbital (almost single occupation) due to strong σ donation from the b_{1g} ligand fragment orbital. The neutral gold species $[Au^{III}(L^\bullet)(L)]$ possesses a very low spin

density of 0.06 at the gold(III) ion. This species carries the spin density of one unpaired electron in a predominantly ligand-based $2b_{2g}$ orbital with only 8% (from Löwdin population) metal d character.

In contrast, the spin density at the central nickel ion in $[Ni(L)(L^\bullet)]^-$ is larger at 0.31 indicating an enhanced Ni(III) character in this species. The corresponding spin densities at the central palladium and platinum ion in $[M^{II}(L)(L^\bullet)]^-$ complexes are between those of the nickel and gold case at 0.16 and 0.21, respectively.

(d) Calculation of EPR Parameters. Table 9 compares the calculated EPR g-values with the experimental ones for the $[M(L)(L^\bullet)]^z$ complexes of Ni, Pd, and Pt with $z = 1-$ and of Au with $z = 0$. Table 10 shows the individual isotropic spin−dipolar and spin−orbit coupling contributions to the metal HFC tensor.

As shown above, all of these species possess a common $^2B_{2g}$ ground state with an unpaired electron in the predominantly ligand-based $2b_{2g}$ orbital. Since this SOMO transforms "gerade" upon inversion, it can mix with the out-of-plane metal d_{xz} orbital whereby it acquires some metal character (Table 7). This metal character gives rise to sizable first-order dipolar metal hyperfine coupling. It also enhances the spin-polarization of the metal core which is responsible for the isotropic Fermi contact contribution to the hyperfine coupling constant. Furthermore, the $^2B_{2g}$ ground state readily

Table 9. Experimental {for $[M(L^{Bu})(L^{Bu\bullet})]^n$ Complexes} and (in Parentheses) Calculated {for $[M(L)(L^\bullet)]^n$ Complexes} EPR Parameters Obtained from the Scalar Relativistic ZORA-B3LYP DFT Methods Using Large Uncontracted Gaussian Bases at the Metal and Uncontrated All Electron Polarized Triple-ξ (TZVP) Gaussian Bases for the Remaining Atoms[a]

complex	g_x	g_y	g_z	A_x,[b] MHz	A_y,[b] MHz	A_z,[b] MHz	W_x,[c] G	W_y,[c] G	W_z,[c] G
$[Ni^{II}(L)(L)]^-$	2.05 (2.07)	2.18 (2.19)	2.01 (2.02)	- (−25)[a]	- (32)[a]	- (−37)[a]	7	30	8
$[Pd^{II}(L)(L)]^-$	2.03 (2.04)	2.03 (2.05)	2.01 (1.98)	- (11)[a]	- (37)[a]	- (11)[a]	75	104	54
$[Pt^{II}(L)(L)]^-$	2.06 (2.06)	2.21 (2.13)	1.83 (1.91)	320 (−302)	278 (−210)	227 (−129)	30	36	44
$[Au^{III}(L)(L)]^0$	2.07 (2.04)	2.03 (2.03)	1.91 (1.95)	- (−16)[a]	- (−21)[a]	- (−17)[a]	30	62	44

[a] Fermi contact, dipolar, and metal spin−orbit contributions to the hyperfine coupling are included in the calculations.

Table 10. Calculated Contributions of the Isotropic Fermi-Contact, Anisotropic Dipolar, and Second-Order Orbital Terms to the Hyperfine Coupling Parameters in the $[M(L)(L^\bullet)]^n$ Complexes As Obtained from the Scalar Relativistic ZORA-B3LYP DFT Methods Using Large Uncontracted Gaussian Bases at the Metal and Uncontracted All Electron Polarized Triple-ξ (TZVP) Gaussian Bases for the Remaining Atoms

complex	A_{iso}, MHz	A_{Dip}, MHz			A_{Orb}, MHz			$A_{Tot.}$, MHz		
		x	y	z	x	y	z	x	y	z
$[Ni^{II}(L)(L)]^-$	31	−45	79	−31	−11	−78	−37	−25	32	−37
$[Pd^{II}(L)(L)]^-$	26	−13	22	−11	−2	−11	−4	11	37	11
$[Pt^{II}(L)(L)]^-$	−355	272	23	127	−219	122	99	−302	−210	−129
$[Au^{III}(L)(L)]^0$	−22	3	-5	2	3	6	3	−16	−21	−17

mixes with relatively low-lying d−d excited states thereby giving rise to a sizable orbital angular momentum which contributes to the hyperfine coupling as well as to the g-shifts in the EPR spectra. From Table 10 it is obvious that all three contributions are of comparable magnitude in the $[M(L)(L^\bullet)]^z$ complexes but partially cancel each other. Experimental HFC numbers are only available for the Pt complex where the calculations appear to give a reasonable result. The remaining errors are still sizable as expected from the complexity of the task (note that the sign of the HFC values is not known from experiment). As pointed out above, in $[Au^{III}(L^\bullet)(L)]^0$ there is little mixing (8%) of the Au d_{xz} orbital in the $2b_{2g}$ SOMO because the d manifold is low-lying in energy due to the large effective nuclear charge of Au^{III}. Together with the rather small nuclear moment of the ^{197}Au nucleus, HFC's of only −16, −21, and −17 MHz are calculated which would fall well within the line width of the experiment.[8] There is also little angular momentum in the ground-state wave function, and thus, the calculated and observed g-shifts are small and reflect the organic radical character of the ground state.

$[Ni^{II}(L)(L^\bullet)]^-$ represents the case of the highest back-bonding interaction (Z_{eff} of Ni(II) being the lowest in energy in the present series) with a metal character of 34% in the SOMO (31% d-orbital spin population from NPA). The calculated g-shift is relatively large at $\Delta g \sim 0.15$ in full agreement the experimental results. Calculated ^{61}Ni hyperfine splittings of −25, +32, and −37 MHz are also in qualitative agreement with values reported for related complexes (NR_4)-$[Ni(S_2C_2(CN)_2)_2]$ (−15, 38, −12 MHz)[32] and $(NR_4)[Ni$-$(xylene-1,2-dithiolate)_2]$ (9, 46, 6 MHz).[33]

For $[Ni(L^{Bu\bullet})(L^{Bu})]^-$ ^{61}Ni HFCs of $A_1(^{61}Ni) = 16$, $A_2(^{61}Ni) < 5$, and $A_3(^{61}Ni) = 40$ MHz have been observed[7] in good agreement with the calculated ones for $[Ni(L^\bullet)(L)]^-$. The calculated EPR parameters for $[Pd^{II}(L)(L^\bullet)]^-$ agree also well with experiment; a small metal contribution of 21% of the SOMO (16% d-orbital spin population from NPA) gives rise to only small HFCs. For the $[Pt^{II}(L)(L^\bullet)]^-$ species the calculated ^{195}Pt hyperfine splittings are in acceptable agreement with experiment, but the calculated g_y and g_z compo-

nents are somewhat under- and overestimated, respectively, probably reflecting the limitations of the simple semiempirical spin−orbit operator used in this study. The metal contribution to the $2b_{2g}$ SOMO is 24% (21% d-orbital spin population from NPA).

(d) Optical Spectra. The optical electronic spectra of $[M(L_N)_2]^n$ and $[M(L_{N,O})_2]^n$ complexes, where M = Ni, Pd, and Pt, $n = 0$ and $1-$, and L_N represent an o-phenylenedia-mide or an o-amidophenolate ($L_{N,O}$) ligand, have been studied experimentally and by DFT calculations.[9] The analysis showed that the very intense absorption maximum in the near-infrared (NIR) region of the monoanions corresponds to an intervalence charge-transfer transition (IVCT) of the type $(L)M(L^\bullet) \leftrightarrow (L^\bullet)M(L)$. In the spectra of the present benzene-1,2-dithiolato monoanionic complexes **1a−3a** these intense IVCT are also observed (Figures 5 and 11). Their positions and intensities are dependent on the nature of the central metal ion (Table 4).

For the paramagnetic $[M(L)(L^\bullet)]^z$ complexes there are 4 spin and electric dipole allowed transitions from the seven doubly occupied MOs in Figure 10 into the singly occupied $2b_{2g}$ and virtual $1b_{1g}$ orbitals expected. The low-energy $1b_{1u} \rightarrow 2b_{2g}$ and $1a_u \rightarrow 2b_{2g}$ transitions are IVCTs in origin with the former expected to be more intense (x-polarized $^2B_{1u}$ state) than the latter (y-polarized ^2A_u state). The third allowed $1a_u \rightarrow 1b_{1g}$ transition (ligand-to-metal charge transfer (LMCT) in character) leads to *two* $^2B_{3u}$ and one $^4B_{3u}$ states. Note that in the excited state there are three unpaired electrons which can spin couple to two doublets and one quartet state. The transitions to the $^2B_{3u}$ states are allowed in z-polarization. However, the second $^2B_{3u}$ component corresponds to a double excitation and should have no intensity on its own. The two $^2B_{3u}$ states may interact, and the "dark" component may borrow intensity from the "bright" one. As pointed out previously,[9] a single determinant description for the complexes is an oversimplification and not appropriate for such a complicated spin-coupling system in the excited states. Therefore, we will limit the description of the electronic structure of these complexes to the two IVCT bands in the time-dependent DFT calculations. This appears even more
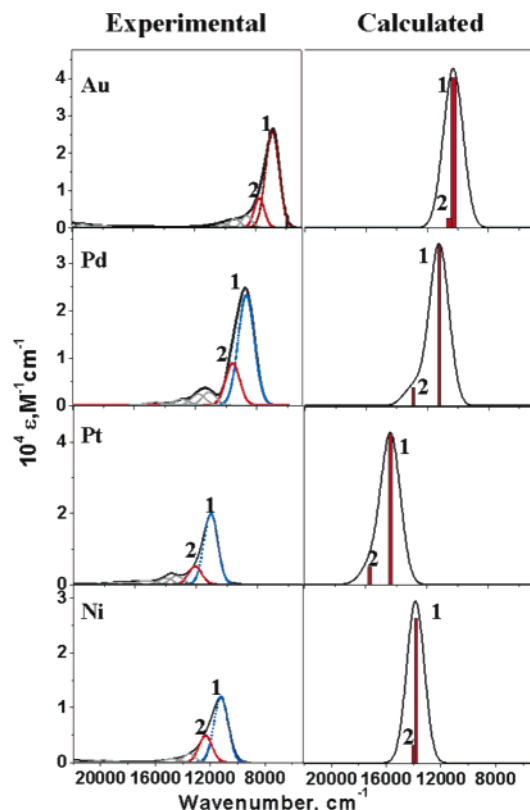
Figure 11. Experimental and calculated absorption spectra for [M(L)-(L•)]^z species. The experimental values are for complexes **4**, **2a**, **3a**, and **1a** (from top to bottom) containing 3,5-di-*tert*-butylbenzene-1,2-dithiolate ligands.

justified as the components of the $1a_u \rightarrow 1b_{1g}$ transition are expected to appear at rather high energies. They do not appear in the calculated first 25 (energy range 5000−25 000 cm^{-1}) states for these complexes.

The room-temperature absorption spectra of **1a**, **2a**, **3a**, and **4** in CH$_2$Cl$_2$ have been subjected to a Gaussian deconvolution (20 000−5000 cm^{-1}). The results are summarized in the Supporting Information Table S1. In each case the spectrum is dominated by two intense transitions labeled 1 and 2 in Figure 11 followed by some weaker transitions which most probably correspond to d−d transitions. Bands 1 and 2 are assigned to the IVCT transitions $1b_{1u} \rightarrow 2b_{2g}$ and $1a_u \rightarrow 2b_{2g}$, respectively. The experimental transition energies are found to be in reasonable agreement with the calculated ones given in Table 11. Both are dependent on the nature of the central metal ion and show a

trend of decreasing energy and increasing intensity on going from the Ni to the Pt, to the Pd, and, finally, to the Au species. The origin of this behavior may be traced back to the relative energies of the donor and the acceptor orbitals of the IVCT states. The main reason for the splitting of the energies of the $1b_{1u}$ and the $2b_{2g}$ orbitals is attributed to the strength of the interaction of the ligand b_{2g} combination with the metal d_{xz} orbital. Since this interaction is antibonding, it raises the energy of the $2b_{2g}$ orbital with respect to the $1b_{1u}$. An increase of the energy of the metal d orbitals will bring them closer in energy to the ligand orbitals, and superexchange through the central metal ion will be more effective yielding an increased destabilization of the $2b_{2g}$ level with respect to the $1b_{1u}$ and $1a_u$ levels. A blue shift of the IVCT bands results. In the present paramagnetic complexes **1a**, **2a**, **3a**, and **4** the variation of the effective nuclear charge combined with relativistic effects at the respective central metal ion increases the energy of the nd orbitals in the following order: Au < Pd < Pt < Ni. Accordingly, the calculated energies of the IVCT bands increase on going from **4** to **2a**, to **3a**, and to **1a** in excellent agreement with experiment (Figure 11).

3. Diamagnetic [M(L)$_2$]^z Species (M= Ni, Pd, Pt, z = 2−; Cu, Au, z = 1−). (a) Geometry. The calculated structures for [M(L)$_2$]^z [M = Ni, Pd, Pt ($z = 2-$); M = Cu, Au ($z = 1-$)] feature long C−S bond distances at an average of 1.77 Å. The C−C bond lengths within the phenyl rings are essentially equivalent at an average distance of 1.403 Å. This indicates the presence of two closed-shell benzene-1,2-dithiolate(2−) ligands in each complex rendering the oxidation state +II for the Ni, Pd, and Pt complexes and +III for the Au species (nd^8, $S_{Metal} = 0$).

(b) Bonding. Upon one-electron reduction of the [M(L•)-(L)]^z species the additional electron enters the $2b_{2g}$ orbital which becomes the HOMO of these reduced species. The calculated ground-state electronic configuration is therefore the following: $(1a_g)^2(2a_g)^2(1b_{3g})^2(1b_{2g})^2(1a_u)^2(2b_{3g})^2(1b_{1u})^2$-$(2b_{2g})^2(1b_{1g})^0$. This reduction process is accompanied by an increase in the metal character of the $2b_{2g}$ orbital (Table 7), but the composition of the LUMO remains unaltered. The natural population analysis for the diamagnetic [M(L)$_2$]^z complexes reveals nearly identical nd populations as has been established for their paramagnetic counterparts [M(L•)(L)]^z (Table 8). It is therefore appropriate to describe these [M(L)$_2$]^z species as Ni^{II}, Pd^{II}, Pt^{II}, Cu^{III}, and Au^{III} complexes

Table 11. Analysis of the Intervalence Charge Transfer Bands in the [M(L)(L•)]^z Complexes Following Gaussian Deconvolution of the Experimental Data (in CH$_2$Cl$_2$ Solution for [M(L^{Bu})(L$^{Bu•}$)]^z Complexes) Shown in Figure 11 Combined with the Results of the Scalar Relativistic ZORA-B3LYP TD-DFT Calculation in Vacuum Using Large Uncontracted Gaussian Bases at the Metal and Uncontracted All Electron Polarized Triple-ξ (TZVP) Gaussian Bases for the Remaining Atoms

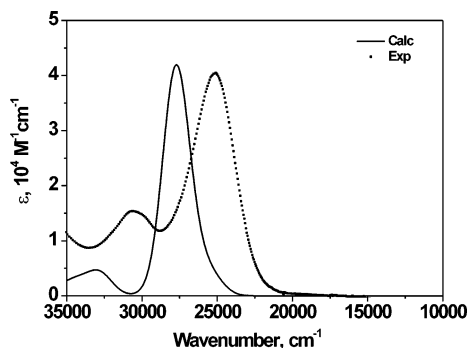|		energy, cm^{-1}		oscillator strength	
complex	transition	expt	calcd	expt	calcd
[Au^{III}(L)(L)]	$1b_{1u} \rightarrow 2b_{2g}$	7 112	10 260	0.122	0.277
	$1a_u \rightarrow 2b_{2g}$	7 800	10 570	0.028	0.019
[Pd^{II}(L)(L)]$^-$	$1b_{1u} \rightarrow 2b_{2g}$	8 874	11 220	0.131	0.236
	$1a_u \rightarrow 2b_{2g}$	9 750	12 905	0.044	0.031
[Pt^{II}(L)(L)]$^-$	$1b_{1u} \rightarrow 2b_{2g}$	11 320	14 358	0.105	0.292
	$1a_u \rightarrow 2b_{2g}$	12 300	15 732	0.023	0.032
[Ni^{II}(L)(L)]$^-$	$1b_{1u} \rightarrow 2b_{2g}$	11 231	13 819	0.065	0.182
	$1a_u \rightarrow 2b_{2g}$	12 372	14 017	0.025	0.023

Figure 12. Electronic spectrum of **5** in CH₂Cl₂ solution at 25 °C (solid line, experimental spectrum; broken line, calculated spectrum): (a) hyperfine splitting experimentally not observed; (b) sign of the hyperfine coupling parameters not determined experimentally; (c) experimental line width.

with an nd^8 electron configuration ($S_M = 0$) and two closed-shell benzene-1,2-dithiolate ligands. The DFT calculations on the $[Cu^{III}(L)_2]^-$ species are in excellent agreement with those reported for $[Cu^{III}(pdt)_2]^-$, where pdt^{2-} represents the dianion of pyrazine-2,3-dithiol.[16] These and the previous calculations clearly rule out an electronic structure as in $[Cu^{II}(L)(L^•)]$.[14]

(c) Optical Spectra. Due to the double occupancy of the $2b_{2g}$ HOMO there is only one spin and electric dipole allowed $1a_u \rightarrow 1b_{1g}$ transition in these $[M(L)_2]^z$ species. This is a LMCT transition to the vacant d_{xy} orbital which is to be expected at a higher energy ($\sim 25\,000$ cm^{-1}). Since intense transitions in the near-infrared region are absent, the expected d−d transitions cannot borrow intensity from them and, hence, they are not observed in the experimental spectra.

The calculated absorption spectra for the $[Cu^{III}(L)_2]^-$ species is found to be in reasonable agreement with the experiments (Figure 12). The band at 363 nm (experimental 398 nm) is ligand-to-metal charge transfer (LMCT) in character. The other band at 343 nm (experimental 303 nm) is probably an intraligand n → π* ligand transition. The fact that no intense IVCT bands are observed >400 nm is a clear indication that the electronic structure is compatible only with an electronic structure as in $[Cu^{III}(L^{Bu})_2]^-$. Note the difference between the spectra of the monoanions $[Cu(L^{Bu})_2]^-$ in Figure 12 and $[Ni(L^{Bu•})(L^{Bu})]^-$ in Figure 5 (top).

4. Diamagnetic, Neutral $[M(L^•)_2]$ Species (M = Ni, Pd, Pt). (a) Geometry from DFT. The DFT-calculated geometries of the diamagnetic neutral molecules $[M^{II}(L^•)_2]$ are in excellent agreement with the notion that the metal ions are divalent (nd^8, $S = 0$) and S,S-coordinated to two equivalent 1,2-dithiosemiquinonate(1−) ligands. The average C−S bond length at 1.74 Å is short, and the six-membered rings exhibit each two alternating relatively short C−C bonds (C₃−C₂; C₄−C₅) at 1.382 Å and four longer ones at an average 1.415 Å. The overall effect of this quinoidal distortion is small.

(b) Bonding from DFT. In the $[M^{II}(L^•)_2]^0$ species (M = Ni, Pd, Pt) the $2b_{2g}$ orbital is then the LUMO and its metal d_{xz} character is smaller than in the corresponding mono- and dianions (Table 7). The calculated ground state is as follows: $(1a_g)^2(2a_g)^2(1b_{3g})^2(1b_{2g})^2(1a_u)^2(2b_{3g})^2(1b_{1u})^2(2b_{2g})^0$-$(1b_{1g})^0$. The natural population analysis for the $[M^{II}(L^•)_2]^0$ species shows again that the nd^8 electron configuration is

not affected on going from the dianionic to the monoanionic and to the neutral form.

(c) Ab initio Calculations. It has recently been shown[9] that the neutral, diamagnetic square planar complex $[Ni^{II}(L_N^{ISQ})_2]$, where $(L_N^{ISQ})^-$ represents the o-diiminobenzosemiquinonate(1−) π radical, is best viewed as a central low-spin Ni(II) ion (d⁸, $S_{Ni} = 0$) coordinated by two benzo-semiquinonate(1−) ligands (singlet diradical). This means that a single determinant closed-shell description is not an appropriate starting point for a quantitative description of the system. As we show here, the same is true for complexes $[M^{II}(L^•)_2]^0$ (M = Ni, Pd, Pt). A description on a quantitative level using correlated ab initio electronic structure methods has been developed previously[9] and is used here.

We use the spectroscopy oriented configuration interaction (SORCI)[13] method to compute the electronic properties of the $[M^{II}(L^•)_2]^0$ (M = Ni, Pd, Pt) complexes. The SORCI formalism is not restricted to species where a single determinant is dominating the wave function but is a genuine multiconfigurational ab initio method. On the basis of a CAS-(2,2) reference space, which is the minimum required to properly describe a diradical situation with two unpaired electrons, the SORCI method explicitly includes up to quadruple excitations from the closed-shell determinant. These high excitations are required to properly capture the differential dynamic correlation effects. This is particularly important to describe the balance between the ground-state determinant and the contributions of the $(1b_{1u})^2(2b_{2g})^0 \rightarrow (1b_{1u})^0(2b_{2g})^2$ double excitation properly. The relative weights of these two configurations determine the amounts of the ionic and neutral character in the ground-state wave function which is used to estimate the diradical character from[9]

$$\% \text{ diradical} = 200\sqrt{\frac{c_0^2 c_d^2}{c_0^2 + c_d^2}} \qquad (3)$$

where c_0^2 and c_d^2 are the weights of the closed-shell determinant and the double excitation in the final CI wave function. Furthermore, the SORCI method allows for the calculation of more accurate transition energies for the $(1b_{1u})^2(2b_{2g})^0 \rightarrow (1b_{1u})^1(2b_{2g})^1$ single and $(1b_{1u})^2(2b_{2g})^0 \rightarrow (1b_{1u})^0(2b_{2g})^2$ double excitations in $[M(L^•)_2]$ complexes with M = Ni, Pd, and Pt than is possible within a DFT framework. Third, the singlet−triplet energy gaps ($-2J_{GS}$) can also be calculated on the basis of pure spin wave functions which in turn give the estimation of the ground-state effective exchange coupling constants $J_{GS}(H_{ex} = -2J_{GS}\mathbf{S_a}\cdot\mathbf{S_b})$ in the above complexes.

Since we are dealing with heavy metals, scalar relativistic effects were included in the calculations using the ZORA method. The results of the scalar relativistic ZORA-SORCI calculations for the $[M(L^•)_2]$ species with M = Ni, Pd, and Pt are summarized in Table 12. To put the present results into perspective, we have also calculated the corresponding quantities for the $[Ni(L_N^{ISQ})_2]$ and $[Ni(L_O^{SQ})_2]$ complexes

Table 12. Calculated (ZORA-SORCI) Absorption Spectra of the $[M(L^\bullet)_2]$, $[M(L_N^{ISQ})_2]$, and $[M(L_O^{ISQ})_2]$ Species and Their Comparison with the Experiments

complex	singlet–triplet gap, cm^{-1}	% diradical	LLCT energy, cm^{-1}		$10^3 f_{osc}$	
			calcd	expt	calcd	expt
$[Ni(L)_2]^0$	9734	32	10 266	11 508[a]	403	135[a]
$[Pd(L)_2]^0$	5799	50	12 851	11 326[a]	464	265[a]
$[Pt(L)_2]^0$	10423	30	15 716	12 669[a]	635	208[a]
$[Ni(L_N^{ISQ})_2]^0$	5019	48	13 584	12 660[b]	611	287[b]
$[Ni(L_O^{SQ})_2]^0$	1397	78	13 516	10 890[c]	318	∼64[c]

[a] Experimental values obtained in CH_2Cl_2 solutions for complexes involving the 3,5-di-*tert*-butyl-1,2-benzenedithiolate ligands. [b] From ref 9. [c] Measured in hexane (Lange, C. W.; Pierpont, C. G. *Inorg. Chim. Acta* **1997**, *263*, 21). The oscillator strength was estimated from the published extinction coefficient by assuming the same band shape as in ref 9 for the corresponding nitrogen complex.

using the same methods and basis sets.[43] The singlet–triplet separation is found to be larger in the $[M(L^\bullet)_2]$ complexes as compared to that in the $[M(L_N^{ISQ})_2]$ and $[M(L_O^{SQ})_2]$ complexes, which is reflected in the lower diradical character in the former complexes. On the basis of our previous estimates of the singlet–triplet gap in $[M(L_N^{ISQ})_2]$ of ∼3100 cm^{-1}, the present calculations appear to overestimate the singlet–triplet separation by ∼0.2 eV. The chemical trends from the present calculations are nevertheless believed to be reliable.

The results obtained for the composition of the singlet ground-state wave function and the diradical character are compatible with the comparative capability of the ligands in the two cases to stabilize the unpaired π electrons by delocalization over the phenyl rings. This delocalization is determined by the semiquinone character of the ligands, which is related to the capability of the N and S atoms to form double bonds with the phenyl rings. This double bond forming tendency increases on going from S to N donor atoms. The weak double bond forming tendency of S atoms is also reflected in the relatively large accumulated spin density (53%, Figure 9) at the S atoms of $(L^\bullet)^-$.

The intense near-IR transition in a large variety of metal dithiolene complexes had been interpreted earlier as simple HOMO–LUMO transitions.[11,12] As has been explained previously,[9] this interpretation is valid only if the ground-state wave functions for the complexes contain equal contributions from the ionic and the neutral terms, i.e., for complexes with a diradical index of zero. However, in the present case, the diradical index for the $[M(L^\bullet)_2]$ complexes is found to be too high (Table 12) to assign their intense near-IR transitions as simple HOMO–LUMO transitions. They should rather be interpreted as LLCT transitions.

The SORCI calculations show increasing diradical character and a decreasing singlet–triplet $(-2J_{GS})$ energy gap on going from the platinum to the nickel and to the palladium species (Table 12). Thus, the results of the present analysis show that the antiferromagnetic interaction between radicals

through the central palladium is weaker than through nickel, whereas the interaction through the central platinum is the strongest in the series. Similar trends were also obtained for the $[M(L_N^{ISQ})_2]$ species.[9]

The experimental absorption spectrum of the $[M(L^\bullet)_2]$ species with M = Ni, Pd, and Pt between 5000 and 20 000 cm^{-1} together with a Gaussian fit is shown in the Supporting Information Figure S1. The results are summarized in the Supporting Information Table S2. It is evident that more than one absorption band is required to fit the experimental spectrum in each case. However, the spectrum is strongly dominated by an intense transition LLCT band (11 508 cm^{-1} for Ni, 11 326 cm^{-1} for Pd, 12 669 cm^{-1} for Pt) in each case, followed by some weaker bands. As explained earlier, these low-intensity bands probably correspond to a complicated series of d–d transitions with varying spin coupling to the open-shell ligands; they are not taken care of in the present SORCI calculations.

As evident from Table 12, the calculated transition energies are found to be in reasonable agreement with the experiments. However, the intensities are unfortunately not well reproduced in the calculations. It is particularly puzzling that the Pt species experimentally has the LLCT intensity between the Ni and Pd case while from qualitative considerations[12] and the ab initio calculations it is expected to have maximum intensity in the whole series.

Conclusions

The electronic structures of square planar complexes containing the diamagnetic dianions **1b**, **2b**, and **3b**, the paramagnetic monoanions **1a**, **2a**, and **3a**, and, finally, the diamagnetic neutral compounds **1**–**3** have been elucidated experimentally and by density functional theory and correlated ab initio methods (SORCI). The most salient features may be summarized as follows:

$[M^{II}(L)_2]^{2-}$ **(M = Ni, Pd, Pt).** These diamagnetic square planar dianions consist of a divalent metal ion (Ni, Pd, Pt) and two S,S-coordinated, closed-shell benzene-1,2-dithiolate-(2−) ligands.

$[M^{II}(L)(L^\bullet)]^-$ **(M = Ni, Pd, Pt).** These square planar, paramagnetic $(S = {}^1/_2)$ monoanions consist of a divalent metal ion (Ni, Pd, Pt; nd^8, $S_M = 0$) and one S,S-coordinated benzene-1,2-dithiolate(2−) ligand as well as one S,S-coordinated benzene-1,2-dithiosemiquinonate(1−) π radical anion. This ligand mixed valency is of class III (delocalized). An intense IVCT band in the NIR is observed in all three

(43) The results of the structure optimization using the BP86/ZORA method for [Ni (L$_O^{SQ}$)$_2$] resulted in excellent agreement with the X-ray structure of [Ni(3,6-di-*tert*-butyl-*o*-benzosemiquinone)$_2$] reported by Abakumov et al. (Abakumov, G. A.; Cherkasov, V. K.; Bubnov, M. P.; Ellert, O. G.; Rakitin, Y. V.; Zakharov, L. N.; Struchkov, Y. T.; Saf'yanov, Y. N. *Bull. Russ. Acad. Sci.* **1992**, *41*, 1813. Translated from: *Izv. Acad. Nauk, Ser. Khim.* **1992**, *10*, 2315) with all metal–ligand and intraligand distances reproduced within 0.02 Å of their experimental values. The compound was reported to be diamagnetic up to 470 K.

cases. The $2b_{2g}$ MO is the SOMO; it contains a small $M(nd_{xz})$ metal character of 34% for the Ni, of 21% for the Pd, of 24% for the Pt, and of only 8% for the $[Au^{III}(L)(L^{\bullet})]^0$ complex.

$[M^{II}(L^{\bullet})_2]$ (M = Ni, Pd, Pt). These square planar diamagnetic neutral compounds consist of a divalent metal ion (Ni, Pd, Pt; nd^8, $S_M = 0$) and two S,S-coordinated 1,2-dithiosemiquinonate(1−) π radical anions. The two spins are intramolecularly, strongly antiferromagnetically coupled via a superexchange mechanism mediated through the diamagnetic metal(II) ion (nd^8, $S_M = 0$). Thus, these species possess 32%, 50%, and 30% singlet diradical character, respectively, as has been deduced from spectroscopy oriented configuration interaction ab initio methods with inclusion of scalar relativistic corrections. At the same level of approximation, the diradical character[9] in the series of square planar neutral bis(dioxolene)nickel(II) complexes decreases on going from two O,O-coordinated semiquinonate(1−) ligands ($\sim$78%), to two N,N-coordinated o-diiminebenzosemiquinonate(1−) ligands ($\sim$48%), to two S,S-coordinated benzene-1,2-dithiolate(1−) ligands (32%). It should be noted that the values of the diradical character apparently depend rather sensitively on the details of the theoretical method as we have found significantly larger values ($\sim$75−80%) for the $[Ni(L_N^{ISQ})_2]^0$ system previously using somewhat different theoretical methods.[9a] However, the diradical character is not a physical observable and its significance is consequently in that it provides insight into the chemical trends along a series. In addition it provides a feeling for the open-shell character of the investigated systems. Similarly, the *calculated* singlet−triplet gaps increase from $\sim$1400 cm^{-1}, to $\sim$5000 cm^{-1}, and to $\sim$9700 cm^{-1} along the same series. The electronic spectra of **1−3** display very intense LLCT bands in the NIR region.

$[M(L)_2]^-$ (M = Cu^{III}, Au^{III}). Both complexes consist of a trivalent metal ion with nd^8 configuration and two S,S-coordinated benzene-1,2-dithiolate(2−) ligands. One electron oxidation yields the mixed-valence neutral species $[Cu^{III}(L)(L^{\bullet})]$ and $[Au^{III}(L^{\bullet})(L)]$, respectively. In contrast, the one-electron reductions are metal-centered and yield $[Cu^{II}(L)_2]^{2-}$ ($S = ^1/_2$) and $[Au^{II}(L)_2]^{2-}$ ($S = ^1/_2$).

Supporting Information Available: Figure S1, showing the Gaussian deconvolution of the experimental absorption spectra of the $[M(L^{Bu\bullet})_2]$ species with M = Ni, Pd, and Pt between 5000 and 20 000 cm^{-1}, Tables S1 and S2, containing the results of the Gaussian deconvolution of the absorption spectra of the $[M(L^{Bu\bullet})(L^{Bu})]^z$ and $[M(L^{Bu\bullet})_2]$ complexes, respectively, in CH$_2$Cl$_2$ solutions, and CIF files, containing the complete listings of the crystallographic details, atom coordinates, bond lengths and angles, thermal displacement parameters, and calculated positional parameters for complexes **2a**, **2b***, and **5′**. This material is available free of charge via the Internet at http://pubs.acs.org.

IC0507565